

1 **Open fires in Greenland in summer 2017: transport,**  
2 **deposition and radiative effects of BC, OC and BrC**  
3 **emissions**

4

5 **Nikolaos Evangeliou<sup>1,\*</sup>, Arve Kylling<sup>1</sup>, Sabine Eckhardt<sup>1</sup>, Viktor Myroniuk<sup>2</sup>,**  
6 **Kerstin Stebel<sup>1</sup>, Ronan Paugam<sup>3</sup>, Sergiy Zibtsev<sup>2</sup>, Andreas Stohl<sup>1</sup>**

7

8 <sup>1</sup>Norwegian Institute for Air Research (NILU), Department of Atmospheric and Climate  
9 Research (ATMOS), Kjeller, Norway.

10 <sup>2</sup>National University of Life and Environmental Sciences of Ukraine, Kiev, Ukraine.

11 <sup>3</sup>King's College London, London, United Kingdom.

12

13 \* Corresponding author: N. Evangeliou ([Nikolaos.Evangeliou@nilu.no](mailto:Nikolaos.Evangeliou@nilu.no))

14

## 15 **Abstract**

16        Highly unusual open fires burned in Western Greenland between 31 July and 21 August  
17 2017, after a period of warm, dry and sunny weather. The fires burned on peat lands that  
18 became vulnerable to fires by permafrost thawing. We used several satellite data sets to  
19 estimate that the total area burned was about 2345 hectares. Based on assumptions of typical  
20 burn depths and emission factors for peat fires, we estimate that the fires consumed a fuel  
21 amount of about 117 kt C and emitted about 23.5 t of black carbon (BC) and 731 t of organic  
22 carbon (OC) including 141 t of brown carbon (BrC). We used a Lagrangian particle  
23 dispersion model to simulate the atmospheric transport and deposition of these species. We  
24 find that the smoke plumes were often pushed towards the Greenland Ice Sheet by westerly  
25 winds and thus a large fraction of the emissions (30%) was deposited on snow or ice covered  
26 surfaces. The calculated deposition was small compared to the deposition from global  
27 sources, but not entirely negligible. Analysis of aerosol optical depth data from three sites in  
28 Western Greenland in August 2017 showed strong influence of forest fire plumes from  
29 Canada, but little impact of the Greenland fires. Nevertheless, CALIOP lidar data showed that  
30 our model captured the presence and structure of the plume from the Greenland fires. The  
31 albedo changes and instantaneous surface radiative forcing in Greenland due to the fire  
32 emissions were estimated with the SNICAR model and the uvspec model from the libRadtran  
33 radiative transfer software package. We estimate that the maximum albedo change due to the  
34 BC and BrC deposition was about 0.007, too small to be measured. The average instantaneous  
35 surface radiative forcing over Greenland at noon on 31 August was 0.03–0.04 W m<sup>-2</sup>, with  
36 locally occurring maxima of 0.63–0.77 W m<sup>-2</sup> (depending on the studied scenario). The  
37 average value is up to an order of magnitude smaller than the radiative forcing from other  
38 sources. Overall, the fires burning in Greenland in summer of 2017 had little impact on the  
39 Greenland Ice Sheet, causing a small extra radiative forcing. This was due to the – in a global  
40 context – still rather small size of the fires. However, the very large fraction of the emissions  
41 deposited on the Greenland Ice Sheet makes these fires very efficient climate forcers on a per  
42 unit emission basis. If the expected future warming of the Arctic produces more severe fires  
43 in Greenland, this could indeed cause albedo changes and thus contribute to accelerated  
44 melting of the Greenland Ice Sheet. The fires burning in 2017 may be a harbinger of such  
45 future events.

46

## 47 **1 Introduction**

48 In August 2017 public media reported unprecedented fire events in Western Greenland  
49 (BBC News, 2017; New Scientist Magazine, 2017). These events were documented with  
50 airborne photographs (SERMITSIAQ, 2017) and satellite images (NASA, 2017b) and raised  
51 public concerns about the effects of climate change and possible impacts of soot emissions on  
52 ice melting. Historically, wildfires have occurred infrequently on Greenland, because three-  
53 quarters of the island is covered by a permanent ice sheet and permafrost is found on most of  
54 the ice-free land (Abdalati and Steffen, 2001). Permafrost, or permanently frozen soil, lies  
55 under a several meters thick “active” soil layer that thaws seasonally. But in certain areas,  
56 where the permafrost layer starts melting, it can expose peat, a material consisting of only  
57 partially decomposed vegetation that forms in wetlands over the course of hundreds of years  
58 or longer. Peatlands, also known as bogs and moors, are the earliest stage in the formation of  
59 coal. Globally, the amount of carbon stored in peat exceeds that stored in vegetation and is  
60 similar in size to the current atmospheric carbon pool (Turetsky et al., 2014). When peatlands  
61 dry, they are often affected by fires burning into the peat layers. Peat fires are difficult to  
62 extinguish and they often burn until all the organic matter is consumed. Smoldering peat fires  
63 already are the largest fires on Earth in terms of their carbon footprint (Turetsky et al., 2014).  
64 For Greenland, it has been suggested that degradation of peat will accelerate towards 2080  
65 (Daanen et al., 2011) and that the area affected by the fires in August 2017 is particularly  
66 vulnerable to permafrost thawing (Daanen et al., 2011).

67 Fires in the high northern latitudes release significant amounts of CO<sub>2</sub>, CH<sub>4</sub>, N<sub>2</sub>O, black  
68 carbon (BC) and organic carbon (OC) and their emissions are often transported into Arctic  
69 regions (Cofer III et al., 1991; Hao et al., 2016; Hao and Ward, 1993; Shi et al., 2015). While  
70 BC is the most strongly light-absorbing component of the atmospheric aerosol (Bond et al.,  
71 2013), a portion of OC compounds has shown strong absorption towards shorter wavelengths  
72 of the electromagnetic spectrum (UV), therefore defined as brown carbon (BrC) (Andreae and  
73 Gelencsér, 2006; Chakrabarty et al., 2010). BC is formed by the incomplete combustion of  
74 fossil fuels, biofuels, and biomass (Bond et al., 2013). BrC is emitted from smoldering fires or  
75 solid fuel combustion (Bond, 2001), from pyrolysis of biomass (Mukai and Ambe, 1986) and  
76 from biogenic emissions of humic substances (Limbeck et al., 2003). Due to their particulate  
77 nature, both BC and OC are important for human health (Lelieveld et al., 2015) and climate  
78 impacts (Myhre et al., 2013). BC has an atmospheric lifetime of 3–11 days (Bond et al.,  
79 2013), while BrC lifetimes are estimated at 5–7 days (Jo et al., 2016), thus facilitating

80 transport over long distances (Forster et al., 2001; Stohl et al., 2006). BC, OC and BrC from  
81 mid-latitude sources can thus reach remote areas such as the Arctic. They absorb solar  
82 radiation in the atmosphere (Feng et al., 2013; Hansen and Nazarenko, 2004), have a  
83 significant impact on cloud formation and also decrease surface albedo when deposited on ice  
84 and snow and can accelerate melting processes (Hansen and Nazarenko, 2004; Wu et al.,  
85 2016). This raises particular concerns about the effect of fires burning in the immediate  
86 vicinity of the Greenland Ice Sheet. If a large fraction of the BC emitted by such fires is  
87 deposited on the ice, these fires may be extremely effective in further enhancing the already  
88 accelerating melting of the Greenland Ice Sheet (AMAP, 2017). BC, OC and BrC emissions  
89 from such high latitude fires may also have a substantial effect on the albedo of sea ice.

90 Here we study transport and deposition of BC, OC and BrC over the Greenland Ice  
91 Sheet from the fires that occurred in Western Greenland in August 2017, which likely  
92 represent the largest fires that have occurred on Greenland in modern times (Figure S 1).  
93 Since the fires occurred in an area entirely lacking ground-based observations, we use satellite  
94 data and a Lagrangian atmospheric dispersion model for our study. Finally, we evaluate the  
95 changes in the albedo of the Greenland Ice Sheet from the respective deposition of BC and  
96 BrC and present instantaneous radiative forcing calculations for these two atmospheric  
97 constituents released from the 2007 fires in Greenland.

## 98 **2 Methods**

### 99 **2.1 Definition of burned area**

100 Remote sensing has been useful for delineating fire perimeters, characterizing burn  
101 severity and planning post-fire restoration activities in different regions. The use of satellite  
102 imaging is particularly important for fire monitoring in remote areas due to difficult ground  
103 access. The method that is presented in this section has been already used to calculate burned  
104 area in the highly-contaminated radioactive forests of Chernobyl (Evangelidou et al., 2014,  
105 2015, 2016). Coordinates of fire locations (hot spots) were downloaded from FIRMS (Fire  
106 Information for Resource Management System) (NASA, 2017a). For the mapping of the  
107 burned area, Sentinel 2A images were used. To delineate fire perimeters and define burn  
108 severity precisely, we used Landsat 8 Operational Land Imager (OLI) (resolution: 30×30 m)  
109 together with Sentinel 1A (resolution: 30×30 m) and Sentinel 2A images (resolution: 30×30  
110 m) (see Table 1) by applying the differenced Normalized Burn Ratio (dNBR) (Key and  
111 Benson, 2006):

112 
$$dNBR = NBR_{pre-fire} - NBR_{post-fire} \quad (\text{Eq. 1})$$

113 Normalized burn ratios for pre- ( $NBR_{pre-fire}$ ) and postfire ( $NBR_{post-fire}$ ) images from  
114 Sentinel 2A can be calculated using radiances for near- and shortwave infrared bands (bands 8  
115 (NIR) and 12 (SWIR2) at 0.835  $\mu\text{m}$  and 2.202  $\mu\text{m}$ , respectively):

116 
$$NBR = \frac{1000 \cdot (NIR - SWIR2)}{NIR + SWIR2} \quad (\text{Eq. 2})$$

117 The methodology of applying a dNBR index to assess the impact of fires has been used in  
118 forests of the Northern and Western USA (French et al., 2008; Key and Benson, 2006) and  
119 elsewhere (Escuin et al., 2008; Sunderman and Weisberg, 2011).

120 The burned severity mosaics were created using Sentinel 2A images corrected for  
121 atmospheric scattering (see Chavez, 1988). Pre- and post-fire images were used to create  
122 cloudless mosaics for the area where the Greenland fires burned. A Maximum Value  
123 Composite (MVC) procedure (Holben, 1986) was used to select pixels from each band that  
124 were not cloud covered and have a high value of Normalized Difference Vegetation Index  
125 (NDVI). To avoid spurious burn severity values, manually delineated fire perimeters were  
126 applied and all areas outside were classified as unburned. We have used common dNBR  
127 severity levels (Key and Benson, 2006) that are presented in Figure 1. The occasionally dense  
128 cloud cover was the main obstacle in reconstructing fire dynamics. As an independent source  
129 of information, active fires from MODIS satellite product MCD14DL (Giglio et al., 2003) are  
130 plotted in Supplemental Information (SI) Figure S 2.

## 131 **2.2 Injection altitudes, assumptions on biomass consumption and emissions** 132 **factors**

133 Injection heights into the atmosphere of the emitted smoke were simulated with version  
134 2 of the Plume Rise Model (PRM) (Paugam et al., 2015) which is implemented in the Global  
135 Fire Assimilation System (GFAS) emission inventory (Rémy et al., 2017). The model  
136 (hereafter referred to as PRMv2) is a further development of PRM (Freitas et al., 2006, 2010)  
137 and has already been used in previous studies of fire events (Evangelidou et al., 2015, 2016).  
138 The model simulates a profile of smoke detrainment for every single fire, from which two  
139 metrics are extracted: (i) a detrainment layer (i.e. where the detrainment rate is > 50% of its  
140 global maximum) and (ii) an injection height (InjH, the top of the detrainment layer). Instead  
141 of using the GFAS product, which uses the same statistics as in the PRMv2 InjH calculation,  
142 we ran the model for every detected fire assuming a 6 h persistence and using the same  
143 conversion factor as Kaiser et al. (2012) to estimate the biomass consumption. PRMv2 mass

144 detrainment profiles are then time integrated and extracted at  $1^\circ \times 1^\circ$  spatial resolution with a  
145 500 m vertical mesh to estimate the 3D distribution of biomass burning smoke injection into  
146 the atmosphere. Figure S 3 (SI) shows for all fires recorded in the MODIS fire product  
147 (Justice et al., 2002) during the fire period (31 July – 21 August 2017) the horizontal  
148 distribution of the median height of the emitted smoke and its integration over the longitude  
149 (right panel). Fires in Greenland showed a maximum injection height of around 2 km, but  
150 according to PRMv2 the majority of the emissions (90%) remained below 800 m. Low  
151 injection heights mostly inside the daytime planetary boundary layer are quite typical for  
152 smoldering fires including peat fires (Ferguson et al., 2003) such as those burning in  
153 Greenland (see below). For modeling the dispersion of BC, OC and BrC released from the  
154 Greenland fires, the emission profiles from PRMv2 were ingested into the Lagrangian particle  
155 dispersion model FLEXPART (see section 2.3).

156 Wildfires in boreal peatlands in the Canadian Arctic and in Alaska typically have  
157 (shallow) burn depths of 1–10 cm and consume  $20\text{--}30 \text{ t C ha}^{-1}$  (Benscoter and Wieder, 2003;  
158 Shetler et al., 2008). The consumed carbon is often re-sequestered in 60–140 years after the  
159 fire (Turetsky et al., 2011; Wieder et al., 2009). Given that fire return intervals can be as short  
160 as 100–150 years in sub-humid continental peatlands (Wieder et al., 2009), and may exceed  
161 2000 years in humid climates (Lavoie and Pellerin, 2007), northern peatlands are generally  
162 resilient to wildfire (Magnan et al., 2012). For example, in peatlands of Northern Russia,  
163 organic matter available for combustion has been estimated to be  $121.8 \text{ t C ha}^{-1}$  for forested  
164 lands and  $21.3 \text{ t C ha}^{-1}$  for non-forested lands (Smirnov et al., 2015). Accordingly, a severe  
165 wildfire that burned within an afforested peatland in the Scottish Highlands during the  
166 summer of 2006 had a mean depth of burn of  $17.5 \pm 2.0 \text{ cm}$  (range: 1–54 cm) and a carbon loss  
167 of  $96 \pm 15 \text{ t C ha}^{-1}$  (Davies et al., 2013). In contrast, tropical peatlands can have deep burn  
168 depths of 40–50 cm and release an average of  $300\text{--}450 \text{ t C ha}^{-1}$  (Page et al., 2015; Reddy et  
169 al., 2015). In the present study, we assume an average amount of organic fuel available for  
170 combustion for the Greenland peat fires of August 2017 of  $100 \text{ t C ha}^{-1}$ , guided by values  
171 suggested in Smirnov et al. (2015).

172 Estimation of the emissions of BC, OC and BrC,  $E_{BC,OC,BrC}$  (kg), was based on the  
173 following formula (Seiler and Crutzen, 1980; Urbanski et al., 2011) using the calculated  
174 burned area  $A$  (ha) and a number of assumptions:

175 
$$E_{BC,OC,BrC} = A \times FL \times \alpha \times EF \quad \text{Eq. 1}$$

176 Here,  $FL$  is the mass of the fuel available for combustion ( $\text{kg C ha}^{-1}$ );  $\alpha$  is the dimensionless  
177 combustion completeness, which was adopted from Hao et al. (2016) for litter and duff fuels  
178 (50%).  $EF$  is the emission factor ( $\text{kg kg}^{-1}$ ), which was assumed to be  $0.20 \text{ g kg}^{-1}$  for BC and  
179  $6.23 \text{ g kg}^{-1}$  for OC for peatland fires (Akagi et al., 2011). Emission factors for BrC are rarely  
180 reported, as BrC is only a fraction of OC. To our knowledge, the only reported emission  
181 factors in the literature for BrC are from forest fires in the United States (Aurell and Gullett,  
182 2013) estimated to be  $1.0\text{--}1.4 \text{ g kg}^{-1}$  (value used here:  $1.2 \text{ g kg}^{-1}$ ). Fuel consumption is  
183 calculated as the product of burned area, fuel loading and combustion completeness  
184 ( $A \times FL \times \alpha$ ).

### 185 **2.3 Atmospheric modeling**

186 The emissions of BC, OC and BrC obtained from Eq. 1 were fed to the Lagrangian  
187 particle dispersion model FLEXPART version 10.2 (Stohl et al., 2005) to simulate transport  
188 and deposition. This model was originally developed for calculating the dispersion of  
189 radioactive material from nuclear emergencies, but since then it has been used for many other  
190 applications (e.g., Fang et al., 2014; Stohl et al., 2011, 2013). The model has a detailed  
191 description of particle dispersion in the boundary layer and a convection scheme to simulate  
192 particle transport in clouds (Forster et al., 2007). The model was driven by hourly  $0.5^\circ \times 0.5^\circ$   
193 operational analyses from the European Centre for Medium-Range Weather Forecasts  
194 (ECMWF). Concentration and deposition fields were recorded in a global domain of  $1^\circ \times 1^\circ$   
195 spatial resolution with three hourly outputs. To capture the spatiotemporal variability of BC,  
196 OC and BrC over the Greenland Ice Sheet, a nested domain with  $0.05^\circ \times 0.05^\circ$  resolution was  
197 used. The simulations accounted for wet and dry deposition, assuming a particle density of  
198  $1500 \text{ kg m}^{-3}$  and a logarithmic size distribution with an aerodynamic mean diameter of  
199  $0.25 \mu\text{m}$  and a standard deviation of 0.3 (Hu et al., 2018; Long et al., 2013). The wet  
200 deposition scheme considers below-cloud and in-cloud scavenging separately based on cloud  
201 liquid water and cloud ice content, precipitation rate and cloud depth from ECMWF, as  
202 described in Grythe et al. (2017).

203 To compare BC and OC concentrations in Greenland due to the emissions of the  
204 Greenland fires to those due to emissions occurring elsewhere, we used the so-called  
205 “retroplume” mode of FLEXPART for determining the influence of other sources. For only a  
206 few receptor points, this mode is computationally more efficient than forward simulations.  
207 Computational particles were tracked 30 days back in time from four receptor regions:  
208 Northwestern ( $-62^\circ\text{E}$  to  $-42^\circ\text{E}$ ,  $72^\circ\text{N}$  to  $83^\circ\text{N}$ ), Southwestern ( $-62^\circ\text{E}$  to  $-42^\circ\text{E}$ ,  $61^\circ\text{N}$  to  $72^\circ\text{N}$ ),

209 Northeastern (-42°E to -17°E, 72°N to 83°N) and Southeastern Greenland (-42°E to -17°E,  
210 61°N to 72°N). The retroplume mode allowed identification of the origin of BC and OC  
211 through calculated footprint emission sensitivities (often also called source-receptor  
212 relationships) that express the sensitivity of the BC and OC surface concentrations at the  
213 receptor to emissions on the model output grid. If these emissions are known, BC and OC  
214 concentrations at the receptor can be calculated as the product of the emission flux and the  
215 emission sensitivity. Also, detailed source contribution maps can be calculated, showing  
216 which regions contributed to the simulated concentration. For the anthropogenic emissions,  
217 we used the ECLIPSE (Evaluating the CLimate and Air Quality ImPacts of ShortlivEd  
218 Pollutants) version 5 (Klimont et al., 2017) emission data set. For the biomass burning  
219 emissions outside Greenland, we used operational CAMS GFAS emissions (Kaiser et al.,  
220 2012). To our knowledge, actual gridded emissions of BrC are not yet available.

#### 221 **2.4 Instantaneous radiative forcing (IRF) calculations**

222 The IRF of the emitted substances of interest were calculated using the uvspec model  
223 from the libRadtran radiative transfer software package (<http://www.libradtran.org/doku.php>)  
224 (Emde et al., 2016; Mayer and Kylling, 2005). The radiative transfer equation was solved in  
225 the independent pixel approximation using the DISORT model in pseudo-spherical geometry  
226 with improved treatment of peaked phase functions (Buras et al., 2011; Dahlback and  
227 Stamnes, 1991; Stamnes et al., 1988). Radiation absorption by gases was taken from the Kato  
228 et al. (1999) parameterization modified as described in the libRadtran documentation and  
229 Wandji Nyamsi et al. (2015). External mixture of aerosols was assumed, i.e. BC and BrC  
230 were treated in isolation of other aerosol types that may also have been present in the plume.  
231 This assumption likely leads to underestimates of the radiative impacts, at least for BC  
232 (Jacobson, 2001), in the atmosphere as coating, for example, can enhance its radiative effects.  
233 However, these assumptions should have little impact on the more important albedo  
234 calculations (see below). For snow-covered surfaces, deposited BC and BrC were assumed to  
235 reside in the uppermost 5 mm. Below 5 mm the snow was assumed to be without any  
236 impurities. The albedo of the snow was calculated with the SNICAR model  
237 (<http://snow.engin.umich.edu/info.html>) in a two-layer configuration (Flanner et al., 2007,  
238 2009).

239 The IRF was calculated for three scenarios: (a) BC only, (b) BC and BrC and (c) BC and  
240 BrC, where all OC is considered to be BrC. The BC only scenario demonstrates the impact of  
241 BC alone, while the two other scenarios provide an estimate of the additional impact of BrC



242 in the plume, with the last scenario considered to be a maximum estimate. We calculated both  
243 the bottom of the atmosphere (BOA) and top of atmosphere (TOA) instantaneous radiative  
244 forcing (IRF) due to the Greenland fires at  $1^\circ \times 1^\circ$  resolution. The IRF includes both the effects  
245 of BC and BrC in the atmosphere and deposited in snow. Note that the IRF does not include  
246 any semi-direct nor indirect effects. We show IRF for cloudy conditions, which represents the  
247 possible radiative effects of BC and BrC due to the 2017 fires with respect to the actual  
248 meteorological situation. Liquid and ice water clouds were adopted from ECMWF.

## 249 **2.5 Remote sensing of the smoke plume**

250 To confirm the presence of the emitted substances from the Greenland fires and  
251 elsewhere in the atmosphere over Greenland, we used the AERONET (AErosol RObotic  
252 NETwork) data (Holben et al., 1998). AERONET provides globally distributed observations  
253 of spectral aerosol optical depth (AOD), inversion products, and precipitable water in diverse  
254 aerosol regimes. We chose data from three stations that were close to the 2017 fires and for  
255 which cloud-free data exist for most of the simulated period, namely Kangerlussuaq  
256 ( $50.62^\circ\text{W}$ – $66.99^\circ\text{N}$ ), Narsarsuaq ( $45.52^\circ\text{W}$ – $61.16^\circ\text{N}$ ) and Thule ( $68.77^\circ\text{W}$ – $76.51^\circ\text{N}$ ). Their  
257 locations are shown in Figure S 2. We used Level 2.0 AOD data (fine and coarse mode AOD  
258 at 500 nm and total AOD at 400 nm) from the AERONET version 3 direct-sun spectral  
259 deconvolution algorithm (SDA version 4.1) product (downloaded on 20 July 2018) for the  
260 simulated period (31 July to 31 August 2017).

261 To examine in particular the vertical depth of the smoke, we used data from the  
262 CALIOP (Cloud-Aerosol Lidar with Orthogonal Polarization) lidar on the CALIPSO (Cloud-  
263 Aerosol Lidar and Infrared Pathfinder Satellite Observations) platform (Winker et al., 2009).  
264 CALIOP provides profiles of backscatter at 532 nm and 1064 nm, as well as the degree of the  
265 linear polarization of the 532 nm signal. For altitudes below 8.3 km lidar profiles at 532 nm  
266 are available with a vertical resolution of 30 m. We have utilized the level 1 data products  
267 (version 3.40) of total attenuated backscatter at 532 nm. This signal responds to aerosols (like  
268 BC, OC and BrC) as well as water and ice clouds, which in most cases can be distinguished  
269 based on their differences in optical properties. The data were downloaded from the ICARE  
270 Data and Services Center (<http://www.icare.univ-lille1.fr/>).

## 271 **3 Results**

### 272 **3.1 Indications of early permafrost degradation and fuel availability**

273 Table 1 reports burned areas in August 2017 calculated for Greenland. In total, 2345  
274 hectares burned between 31 July and 21 August 2017 (Figure 1). We estimate that about 117  
275 kt of carbon were consumed by these fires. The area burned is not large compared to the  
276 global area burned each year (464 million hectares), or the areas burned in boreal North  
277 America (2.6 million hectares) or boreal Asia (9.8 million hectares) (Randerson et al., 2012),  
278 but still highly unusual for Greenland.

279 It is not yet known how these fires started. Fires on carbon-rich soils can be initiated by  
280 an external source, e.g. lightning, flaming wildfire and firebrand, or self-heating. The fires  
281 burned relatively close to the town of Sisimut, so it is quite possible that humans started the  
282 fires. Self-heating is another possibility as porous solid fuels can undergo spontaneous  
283 exothermic reactions in oxidative atmospheres at low temperatures (Drysdale, 2011;  
284 Restuccia et al., 2017b). This process starts by slow exothermic oxidation at ambient  
285 temperature, causing a temperature increase, which is determined by the imbalance between  
286 the rate of heat generation and the rate of heat losses (Drysdale, 2011). Fire initiated by self-  
287 heating ignition is a well-known hazard for many natural materials (Fernandez Anez et al.,  
288 2015; Restuccia et al., 2017a; Wu et al., 2015) and can also occur in natural soils (Restuccia  
289 et al., 2017b). Southwestern Greenland was under anticyclonic influence during the last week  
290 of July and according to the MODIS ESDIS worldview tool, direct sunshine occurred for  
291 eight consecutive days before the fires started at the end of July 2017. It might be possible  
292 that this long period of almost continuous insolation at these latitudes in July heated the soil  
293 enough to self-ignite. In any case, the continuous sunshine had dried the soil, making it  
294 susceptible to fire.

295 The fact that these fires were burning for about three weeks but spread relatively slowly  
296 compared to above-ground vegetation fires indicates that the main fuel was probably peat.  
297 The predominant vegetation in Western Greenland varies from carbon-rich *Salix glauca* low  
298 shrubs (mean canopy height: 95 cm), mainly at low altitude south-facing slopes with deep  
299 soils and ample moisture, to dwarf-shrubs and thermophilous graminoid vegetation (Arctic  
300 steppe) at higher altitudes (Jedrzejek et al., 2013). In addition, the observed smoke was nearly  
301 white, indicating damp fuel, such as freshly thawed permafrost, which produces smoke rich in  
302 OC aerosol (Stockwell et al., 2016).

303 Literally no fires should be expected in Greenland, since there is little available fuel as  
304 it has been suggested by global models and validated by observations (Daanen et al., 2011;  
305 Stendel et al., 2008); the only way to provide substantial amounts of fuel in Greenland is  
306 permafrost degradation. However, it has been suggested that significant permafrost loss in  
307 Greenland may occur only by the end of the 21<sup>st</sup> century (Daanen et al., 2011; Stendel et al.,  
308 2008). The fires in 2017 might indicate that significant permafrost degradation has occurred  
309 sooner than expected.

### 310 **3.2 Transport and deposition of BC in Greenland**

311 We estimate that about 23 t of BC and 731 t of OC, including 141 t of BrC, were  
312 released from the Greenland fires in August 2017 (Table 1). According to the FLEXPART  
313 model simulations, these emissions were transported and deposited as shown in Figure 2. Due  
314 to the low injection altitude of the releases within the boundary layer, transport was relatively  
315 slow and thus the emitted substances initially remained quite close to their source. Slow  
316 transport was also favored by mostly anticyclonic influence during the first half of August. It  
317 seems that even though katabatic winds from the Greenland Ice Sheet occasionally  
318 transported the plume westwards, most of the time the large-scale circulation pushed the  
319 plume back towards Greenland (see SI animations). Consequently, a large fraction of the  
320 emitted substances were deposited in Southwestern Greenland. On 3 August a small portion  
321 of the emitted BC, OC and BrC (0.5 t, 16.1 t and 3.1 t, respectively) were lifted higher into  
322 the atmosphere and were transported to the east and deposited in the middle of the Ice Sheet  
323 over the course of the following two days (4 and 5 August). From 5 to 8 August, when the  
324 fires were particularly intense, the emitted aerosols were transported to the south, where they  
325 were deposited at the southern part of the Ice Sheet and close to the coastline. At the same  
326 time, another branch of the plume was moving to the north depositing BC, OC and BrC over  
327 Greenland's western coastline up to 80°N. Around 10 August, the plume circulated north- and  
328 then eastwards in the northwestern sector of the anti-cyclone and the emitted aerosols were  
329 deposited to the northern part of the Ice Sheet until 13 August. From around 16 August, a  
330 cyclone approached from the northwest and the smoke was briefly transported directly  
331 eastwards along the southern edge of the cyclone (see SI animations). Strong rain associated  
332 with the cyclone's frontal system appears to have largely extinguished the fire by 17 or 18  
333 August, although smaller patches may have continued smoldering for a few more days before  
334 they also died out. The exact fire behavior after 16 August is difficult to determine because of

335 frequent dense cloud cover. However, satellite imagery on 21 August shows no smoke  
336 anymore in the area where the fires had burned.

337 The total deposition of BC, OC and BrC from the fires in Greenland was estimated to  
338 be 9 t, 280 t and 54 t, respectively, or about 39% of the total emissions. About 7 t of BC, 218 t  
339 of OC and 42 t of BrC were deposited on snow or ice covered surfaces, which is equivalent to  
340 30% of the total emissions. Most of the rest was deposited in the Baffin Bay between  
341 Greenland and Canada and in the Atlantic Ocean. With 30% of the emissions deposited on  
342 snow or ice surfaces, Greenland fires may have a relatively large efficiency for causing  
343 albedo changes on the Greenland Ice Sheet.

344 By comparison, the respective BC deposition on snow and ice surfaces over Greenland  
345 from global emissions of BC (from ECLIPSEv5) was only 0.4% (39 kt) of the total emissions.  
346 Even the total deposition of BC in the Arctic ( $>67^{\circ}\text{N}$ ) was only about 3% (215 kt). This  
347 indicates the high relative potential of Greenland fires to pollute the cryosphere (on a per unit  
348 emission basis), likely also giving them a particularly high radiative forcing efficiency.  
349 Considering that the projected rise of Greenland temperatures is expected to result in further  
350 degradation of the permafrost (Daanen et al., 2011) and, hence, likely resulting in more and  
351 larger peat fires on Greenland, this constitutes a potentially important climate feedback which  
352 could accelerate melting of the glaciers and ice sheet of Greenland and enhance Arctic  
353 warming.

354 We also calculated the concentration of the deposited carbon aerosols in Greenland  
355 snow (Figure 3) by taking the ratio of deposited quantities and the amount of water deposited  
356 by rain or snowfall during the same time period (31 July to 31 August 2017). As expected,  
357 snow concentrations show the same general patterns as the simulated deposition with the  
358 highest concentrations obtained close to the source (western side of Greenland). High snow  
359 concentrations were also computed in some regions of the Ice Sheet due to relatively intense  
360 precipitation events. By contrast, dry deposition (example for BC) over the Ice Sheets was  
361 low (Figure S 4). Dry deposition was responsible for a major fraction of the deposition only in  
362 regions where the plume was transported during dry weather, and in most of these regions  
363 total deposition was low. A notable exception is the region close to the fires, where dry  
364 deposition was relatively important due to the generally dry weather when the fires were  
365 burning. It can be also ascribed to the fact that dry deposition occurs in the quasi-laminar sub-  
366 layer close to the surface. A fraction of the aerosols can be quickly deposited close to the  
367 sources before they are transported to higher altitudes and away from the sources (Bellouin

368 and Haywood, 2014). The average calculated snow concentration of BC on the Ice Sheet was  
369 estimated to be  $<1 \text{ ng g}^{-1}$ , but in some areas snow concentrations reached up to  $3 \text{ ng g}^{-1}$ . These  
370 higher values are substantial considering that measured concentrations of BC in snow  
371 typically range up to  $16 \text{ ng g}^{-1}$  in most of Greenland (Doherty et al., 2010) or from  $1 - 17 \text{ ng}$   
372  $\text{g}^{-1}$  in summer 2012 and  $3-43 \text{ ng g}^{-1}$  in summer 2013 (Polashenski et al., 2015) and up to  $15$   
373  $\text{ppb C (ng g}^{-1})$  during preindustrial times (from 1740 to 1870) on average (Legrand et al.,  
374 2016). OC concentrations in snow were  $2 \text{ ng g}^{-1}$  (ppb C), on average, with local maxima of  $10$   
375  $\text{ng g}^{-1}$ . They are lower than those measured in snow over several places in Antarctica ( $23-928$   
376  $\text{ppb C}$ ) (Antony et al., 2011; Grannas et al., 2004; Legrand et al., 2013; Lyons et al., 2007), in  
377 Greenland ( $400-580 \text{ ppb C}$ ) (Grannas et al., 2004) or in the Alps ( $70-304 \text{ ppb C}$ ) (Legrand et  
378 al., 2013). Snow BrC was estimated to be even less; though, to our knowledge, no available  
379 measurements exist in the relevant literature so far.

380 It has been reported that the size of rapidly coagulated aerosol particles produced by  
381 different types of fires ranges between  $0.1$  to  $10 \mu\text{m}$ , but more than 90% of the mass lies  
382 between  $0.1$  and  $1 \mu\text{m}$  (e.g., Conny and Slater, 2002; Long et al., 2013; Zhuravleva et al.,  
383 2017 and many others). Therefore, we simulated the Greenland fires with an aerodynamic  
384 mean diameter of  $0.25 \mu\text{m}$  for BC, OC and BrC and a logarithmic standard deviation of  $0.3$   
385 (see section 2.3), because all these substances have more or less the same lifetimes (Bond et  
386 al., 2013; Jo et al., 2016; Lim et al., 2003). To examine the sensitivity of deposition in the  
387 Greenland Ice Sheet from the Greenland fires of 2017 to the particle size distribution used in  
388 the model, we simulated the same event for particles with aerodynamic mean diameters of  
389  $0.1, 0.25, 0.5, 1, 2, 4$  and  $8 \mu\text{m}$  and calculated the relative standard deviation of deposition  
390 normalized against the aerodynamic mean diameter of  $0.25 \mu\text{m}$  that was our basic  
391 assumption. The results are shown in Figure S 5 for BC. The use of different size distributions  
392 for the BC particles produced from the 2017 fires created a relative uncertainty on the  
393 deposited mass of BC in the Greenland Ice Sheet, which ranges from 10%–30% in 86% of the  
394 Sheet's surface to up to 50% in the rest of the Sheet's surface. As expected, the calculated  
395 uncertainty is sensitive to the use of larger particles for BC; though BC particles larger than  $1$   
396  $\mu\text{m}$  are rather rare in peat fires (Hosseini et al., 2010; Leino et al., 2014).

### 397 **3.3 Impact from other emissions in the Northern Hemisphere**

398 In summertime 2017, intense wildfires were reported in British Columbia, Western  
399 Canada (NASA, 2017c), and fires also burned at mid latitudes in Eurasia, as is typical during  
400 spring and summer (Hao et al., 2016). Previous studies of wildfires have shown that the

401 produced energy can be sufficient to loft smoke above the boundary layer by supercell  
402 convection (Fromm et al., 2005) even up to stratospheric altitudes (Leung et al., 2007). As a  
403 result, emitted aerosols can become subject to long-range transport over long distances  
404 (Forster et al., 2001; Stohl et al., 2007). To examine the impact of these fires in Greenland,  
405 average footprint emission sensitivities were calculated for four compartments of Greenland  
406 (Northwestern, Southwestern, Northeastern and Southeastern Greenland) for the period 31  
407 July to 31 August 2017 and the results are shown in Figure S 6 together with the active fires  
408 in the Northern Hemisphere from 10 July to 31 August 2017 adopted from the MODIS  
409 satellite product (MCD14DL) (Giglio et al., 2003). As can be seen in Figure S 6, fires in  
410 Alaska and in Western Canada might have affected BC, OC and BrC concentrations in  
411 Greenland, as the corresponding emission sensitivities are the highest in North America. On  
412 the contrary, emissions from fires in Eurasia seem to have affected Greenland less.

413         Using gridded emissions for BC and OC, the contribution of both biomass burning and  
414 anthropogenic sources to surface concentrations in the four different regions over Greenland  
415 (Northwestern, Northeastern, Southwestern and Southeastern Greenland, Figure S 7) was  
416 calculated (see section 2.3). Fires affected the northern part of Greenland more than the  
417 southern part with an average BC concentration of about 30 ng m<sup>-3</sup>, almost twice the  
418 respective average for Southern Greenland (≈16 ng m<sup>-3</sup>). OC simulated concentrations were  
419 much higher than those of BC with an average concentration of 945 ng m<sup>-3</sup> in North  
420 Greenland, while the respective concentrations in the southern part were about 490 ng m<sup>-3</sup>.  
421 About one third of BC and OC originated from wildfires in Eurasia and the rest from North  
422 America where the year 2017 appears to have been a particularly high fire year. The  
423 anthropogenic contribution to surface concentrations of BC and OC over Greenland was  
424 between 14% to 50% of the total contribution from all biomass burning sources (Figure S 7),  
425 similar to what has been suggested previously for the Arctic in summer (Winiger et al., 2017).  
426 The anthropogenic contribution is larger in Southern Greenland than in Northern Greenland,  
427 due to the shorter distance from the main emission areas of North America and Western  
428 Europe, but it remains much lower than the biomass burning contribution. The concentrations  
429 of BC and OC that are calculated for the studied fire period (31 July to 31 August 2017) are  
430 relatively high compared to those reported previously. For instance, von Schneidmesser et al.  
431 (2009) observed an annual average BC concentration of 20 ng m<sup>-3</sup> at Summit (Greenland) in  
432 2006, while Massling et al. (2015) reported a summer average BC concentration of 11 ng m<sup>-3</sup>  
433 at station Nord (Greenland) between May 2011 and August 2013. As regards to OC, average

434 concentrations of its water soluble part were measured in 2006 between 194 and 730 ng m<sup>-3</sup> in  
435 Summit, Greenland (Anderson et al., 2008) showing a large decreasing trend compared to  
436 previous years (Dibb et al., 2002). We attribute this difference in the calculated concentrations  
437 to more active fires during 2017 in Greenland than in previous years (see Figure S 1).

438 As an example of the importance of Northern Hemispheric biomass burning emissions  
439 for the air over Greenland, we present time-series of surface BC concentrations in  
440 Northwestern, Northeastern, Southwestern and Southeastern Greenland from the fires in  
441 Greenland and from all the other wildfire emission sources occurring outside Greenland  
442 (North Hemisphere) for the same period of time (Figure 4). The calculated dosages  
443 (concentrations summed over a specific time period) for the same time period were also  
444 computed. The fires in Greenland affected mainly its western part with concentrations that  
445 reached up to 4.8 ng m<sup>-3</sup> (Southwestern Greenland on 10 August) and 4.4 ng m<sup>-3</sup>  
446 (Northwestern Greenland on 12 August), while BC concentrations in the eastern part  
447 remained significantly lower (Figure 4). These concentrations are substantial considering that  
448 the observed surface BC concentrations in Greenland in summer are usually below 20 ng m<sup>-3</sup>  
449 (Massling et al., 2015). Surface BC due to wildfires occurring outside Greenland was also low  
450 most of the time in the studied period (up to 10 ng m<sup>-3</sup> at maximum) except for a large peak  
451 between 19 and 23 August that mainly affected Northern Greenland (Figure 4). The  
452 concentrations during this episodic peak were as high as 27 ng m<sup>-3</sup>. During the same period,  
453 the contribution from anthropogenic emissions was also a few ng m<sup>-3</sup> (Figure 4). BC dosages  
454 for the simulation period (31 July – 10 August 2017) in Western Greenland due to the  
455 Greenland fires were about one order of magnitude smaller than dosages from fires elsewhere  
456 but of the same order of magnitude as BC originating from anthropogenic emissions.

## 457 **4 Discussion**

### 458 **4.1 A validation attempt**

459 There are few observations available that can be used to validate our model results. We  
460 use the AERONET and CALIOP data for some qualitative comparisons. We present only BC  
461 here, but similar plots can be generated for OC, considering that we used the same scavenging  
462 coefficients as for BC to represent the similar lifetimes of BC and OC (Bond et al., 2013; Jo  
463 et al., 2016; Lim et al., 2003). Contours of simulated vertical distribution of BC and column-  
464 integrated simulated BC from fires inside and outside Greenland are plotted together with  
465 time-series of measured AOD (fine and coarse mode AOD at 500 nm and total AOD at 400

466 nm) for the AERONET stations Kangerlussuaq, Narsarsuaq and Thule (Figure 5). It can be  
467 seen that observed AOD variations were in very good agreement with the variation of  
468 simulated column-integrated BC from fires outside Greenland (mainly in Canada), confirming  
469 that the transport of these fire plumes was well captured by FLEXPART. Good examples are  
470 the peaks at Kangerlussuaq on 24 August, at Narsarsuaq on 19 August and at Thule on 21  
471 August (Figure 5) that are attributed to the Canadian fires. The simulated contribution of the  
472 Greenland fires to simulated BC burdens was negligible by comparison, except at  
473 Kangerlussuaq in the beginning of August when the Greenland fire emissions were the  
474 highest. This station is less than 100 km away from where the fires burned, but not in the  
475 main direction of the BC plume transport. It seems the period of simulated fire influence  
476 corresponds to a small increase of the observed AOD values of up to 20% (Figure 5).

477 To validate the smoke plume's vertical extent, we used the CALIOP data. These data  
478 were only available from 5 August 2017 onward and frequent dense cloud cover inhibited  
479 lidar observations at the altitudes below the clouds. High aerosol backscatter was only found  
480 in the close vicinity of the fires. Figure 6a shows NASA's ESDIS view of the plume on 14  
481 August 2017 at 6 UTC (available: [https://worldview.earthdata.nasa.gov/?p=geographic&l=MODIS\\_Aqua\\_CorrectedReflectance\\_TrueColor\(hidden\),MODIS\\_Terra\\_CorrectedReflectance\\_TrueColor,MODIS\\_Fires\\_Terra,MODIS\\_Fires\\_Aqua,Reference\\_Labels\(hidden\),Reference\\_Features,Coastlines&t=2017-08-14&z=3&v=-54.13349998138993,66.35888052399868,-50.32103113049877,69.08420005412792](https://worldview.earthdata.nasa.gov/?p=geographic&l=MODIS_Aqua_CorrectedReflectance_TrueColor(hidden),MODIS_Terra_CorrectedReflectance_TrueColor,MODIS_Fires_Terra,MODIS_Fires_Aqua,Reference_Labels(hidden),Reference_Features,Coastlines&t=2017-08-14&z=3&v=-54.13349998138993,66.35888052399868,-50.32103113049877,69.08420005412792)), where  
485 a clear smoke signal was recorded. A CALIOP overpass through the edge of the plume allows  
486 studying its vertical structure. Increased attenuated backscatter is found below ~1.5 km above  
487 sea level between 52°E and 51°E (Figure 6b; black line denotes the orography). Figure 6c  
488 (red line), shows that the CALIOP overpass transects directly the simulated plume of the  
489 Greenland fires. Notice that the simulated plume also agrees very well with the smoke as seen  
490 in NASA's ESDIS picture (Figure 6a). The vertical distribution of simulated BC as a function  
491 of longitude is illustrated in Figure 6d. It corresponds very well to the vertical distribution of  
492 aerosols observed by CALIOP (Figure 6b). In particular, the smoke resides at altitudes below  
493 1.5 km and at exactly the same location both in the simulations and observations.

#### 495 **4.2 Instantaneous radiative forcing and albedo effects**

496 BOA IRF due to (a) BC only, (b) BC and BrC and (c) BC and BrC when all OC was  
497 assumed to be BrC (extreme scenario) for noon on 31 August 2017 is depicted in Figure 7a–c.  
498 This day is shown because almost all the aerosols emitted by the fires had been deposited,



499 thus giving a high IRF via albedo reduction due to snow contamination. The IRF is the largest  
500 over ice close to the fire site and at locations where relatively large amounts of BC and BrC  
501 were deposited. For BC only, the maximum BOA (TOA) IRF is  $0.63 \text{ W m}^{-2}$  ( $0.59 \text{ W m}^{-2}$ ),  
502 and the average  $0.03 \text{ W m}^{-2}$  ( $0.03 \text{ W m}^{-2}$ ). Including BrC slightly increases the maximum  
503 BOA (TOA) IRF to  $0.65 \text{ W m}^{-2}$  ( $0.61 \text{ W m}^{-2}$ ), while the change in the average IRF values is  
504 negligible. For the extreme BrC scenario, the maximum BOA (TOA) IRF is  $0.77 \text{ W m}^{-2}$  ( $0.71$   
505  $\text{W m}^{-2}$ ) and the average  $0.04 \text{ W m}^{-2}$  ( $0.06 \text{ W m}^{-2}$ ). So, including BrC in our analysis increases  
506 BOA IRF by only 20% even for the extreme scenario.

507 The IRF depends on the optical properties of the smoke from the fire, which are not  
508 known. Hence, a sensitivity analysis was performed where the single scattering albedo (SSA)  
509 was perturbed in contrast to a “medium case” (Figure S 8a) that was adopted from the  
510 SNICAR model (Flanner et al., 2007, 2009) and has been used for the discussion in the  
511 previous paragraph. To estimate the uncertainty due to the choice of BC optical properties,  
512 additional calculations were made by scaling the SSA (red solid lines in Figure S 8a). The  
513 choices of these scaled SSA values were based on the SSA reported for various modified  
514 combustion efficiencies (MCE) by Pokhrel et al. (2016). Pokhrel et al. (2016) reported an  
515 MCE of 0.9 for peat land. As such, our adopted SSA may be considered low (compare black  
516 solid line and red line with upward triangles). Figure S 8b shows the IRF as BC is deposited  
517 for the three cases. It suggests that the IRF ranges between 40% and 130% of our above-  
518 assumed medium-case values for realistic variation of the aerosol optical properties.

519 Figure 7d depicts the temporal behaviour of the cloudy TOA IRF averaged over  
520 Greenland (daily averages) for BC only (red line), for BC and BrC (blue line) and for BC and  
521 BrC, when all OC is assumed to be BrC (black line, extreme case scenario). The daily  
522 averaged IRF is seen to increase as the plume from the fires spreads out and starts to decline  
523 after the fires were extinguished at the end of the month. The fact that the reduction towards  
524 end of August is relatively slow is caused by the effect of the albedo reduction, which persists  
525 until clean snow covers the polluted snow. Overall, albedo reduction dominates the total IRF  
526 averaged over Greenland for the period of study contributing between 85% (in the beginning  
527 of the study period) to 99% (at the end of the study period) and increasing in relative  
528 importance with time as atmospheric BC and BrC are removed. The largest IRF differences  
529 between the BC only case IRF and the two BC+BrC cases occur when there is still smoke in  
530 the air and the lowest IRF differences occur after August 15<sup>th</sup>. This indicates that BrC is most  
531 important for the IRF when it is airborne, even in the extreme scenario. However, for the

532 latter, the impact is also large after August 15<sup>th</sup> due to a further albedo decrease of about  
533 0.001 compared to the case where only BC was considered.

534 According to Hansen et al. (2005) the TOA IRF of BC approximates the adjusted RF as  
535 reported by Myhre et al. (2013). In their Table 8.4, Myhre et al. (2013) estimated the global  
536 averaged RF due to BC between the years 1750 and 2011 to be +0.40 (+0.05 to +0.80) W m<sup>-2</sup>.  
537 Skeie et al. (2011) estimated a global mean radiative forcing of 0.35 W m<sup>-2</sup> due to fossil fuel  
538 and biofuel increases between 1750 and 2000. For Greenland, Skeie et al. (2011) found the  
539 RF to be less than about 0.2 W m<sup>-2</sup>. This number may be compared to our area averaged IRF  
540 estimate due to the Greenland fire. For cloudy conditions the TOA IRF over Greenland due to  
541 the Greenland fires is about a factor 4 to 10 smaller compared with the RF over Greenland  
542 due to BC from all global anthropogenic sources reported in Skeie et al. (2011).

543 The albedo reduction at 550 nm for the three scenarios (BC only, BC+BrC and BC+BrC  
544 extreme) is shown in Figure 7e–g. The maximum albedo change is about 0.006 when only BC  
545 was considered. Adding BrC from the most extreme scenario, the maximum albedo change  
546 was calculated as 0.007 This albedo change has an impact on IRF, but it is too small to be  
547 measured by satellites. For example, MODIS albedo estimates have been compared to in situ  
548 albedo measurements in Greenland by Stroeve et al. (2005). They found that the root mean  
549 square error between MODIS and in situ albedo values was ±0.04 for high quality flagged  
550 MODIS albedo retrievals. Unmanned Aerial Vehicle (UAV) measurements over Greenland  
551 made by Burkhart et al. (2017) have uncertainties of similar magnitude. Also, Polashenski et  
552 al. (2015) reported that the albedo reduction due to aerosol impurities on the Greenland Ice  
553 Sheet in 2012–2014 period is relatively small (mean 0.003), though episodic aerosol  
554 deposition events can reduce albedo by 0.01–0.02. The albedo changes due to BC and BrC  
555 from the Greenland fires are generally an order of magnitude smaller (Figure 7e–g) and thus  
556 too small to be detected by present UAV and satellite instruments and retrieval methods  
557 (Warren, 2013).

## 558 **5 Conclusions**

559 We studied atmospheric transport, deposition and impact of BC, BrC and OC emitted as  
560 a result of unusual open fires burning in Greenland between 31 July and 21 August 2017. Our  
561 conclusions can be summarized below:

- 562 • The fires burned on peat lands that became vulnerable by permafrost thawing. The region  
563 where the fires burned was identified previously as being susceptible to permafrost

564 melting; however, large-scale melting was expected to occur only towards the end of the  
565 21<sup>st</sup> century. The 2017 fires show that at least in some locations substantial permafrost  
566 thawing is already occurring now.

- 567 • The total area burned was about 2345 hectares. We estimate that the fires consumed a fuel  
568 amount of about 117 kt C and emitted about 23.5 t of BC and 731 t of OC including 141 t  
569 of BrC.
- 570 • The Greenland fires were small compared to fires burning at the same time in North  
571 America and Eurasia, but a large fraction of BC, OC and BrC emissions (30%) was  
572 deposited on the Greenland Ice Sheet.
- 573 • Measurements of aerosol optical depth at three sites in Western Greenland in August 2017  
574 were strongly influenced by forest fires in Canada burning at the same time, but the  
575 Greenland fires had an observable impact doubling the column-integrated BC  
576 concentrations at the closest station.
- 577 • A comparison of the simulated BC releases in FLEXPART with the vertical cross-section  
578 of total attenuated backscatter (at 532 nm) from CALIOP lidar showed that the  
579 spatiotemporal evolution and particularly the top height of the plume was captured by the  
580 model.
- 581 • We estimate that the maximum albedo change due to the BC deposition from the  
582 Greenland fires was about 0.006, whereas adding deposited BrC increases albedo to 0.007  
583 at maximum, which is too small to be measured. The average instantaneous BOA radiative  
584 forcing over Greenland at noon on 31 August was between 0.03–0.04 W m<sup>-2</sup> for the three  
585 scenarios (BC only, BC+BrC and BC+BrC extreme), with locally occurring maxima of  
586 0.63 W m<sup>-2</sup>, 0.65 W m<sup>-2</sup> and 0.77 W m<sup>-2</sup>, respectively. The average value when only BC  
587 was considered is up to an order of magnitude smaller than the radiative forcing due to BC  
588 from other sources.
- 589 • We conclude that the fires burning in Greenland in summer of 2017 had small impact on  
590 on the Greenland Ice Sheet, causing almost negligible extra radiative forcing. This was  
591 due to the – in a global context – still rather small size of the fires.

592 The very large fraction of the emissions deposited on the Greenland Ice Sheet (30% of  
593 the emissions) makes these fires very efficient climate forcers on a per unit emission basis.  
594 Thus, while the fires in 2017 were still relatively small on a global scale, if the expected future  
595 warming of the Arctic (IPCC, 2013) produces more and larger fires in Greenland (Keegan et

596 al., 2014), this could indeed cause substantial albedo changes and thus contribute to  
597 accelerated melting of the Greenland Ice Sheet.

598

599 *Data availability.* All data used for the present publication can be obtained from the  
600 corresponding author upon request.

601

602 *Competing financial interests.* The authors declare no competing financial interests.

603

604 *Acknowledgements.* This study was partly supported by the Arctic Monitoring and  
605 Assessment Programme (AMAP) and was conducted as part of the Nordic Centre of  
606 Excellence eSTICC (Nordforsk 57001). We acknowledge the use of imagery from the NASA  
607 Worldview application (<https://worldview.earthdata.nasa.gov/>) operated by the  
608 NASA/Goddard Space Flight Center Earth Science Data and Information System (ESDIS)  
609 project. We thank Brent Holben and local site managers for their effort in establishing and  
610 maintaining the AERONET sites used in this investigation. We thank NASA/CNES engineers  
611 and scientists for making CALIOP data available. The lidar data were downloaded from the  
612 ICARE Data and Service Center.

613

614 *Author contributions.* NE performed the simulations, analyses, wrote and coordinated the  
615 paper. AK performed the radiation calculations and wrote parts of the paper. VM and SZ  
616 performed GIS analysis for the burned area calculations. RP made all the runs for the  
617 injection height calculations using the PRMv2 model. KS analysed satellite data for AOD and  
618 CALIOP, SE and AS commented and coordinated the manuscript. All authors contributed to  
619 the final version of the manuscript.

620

## 621 **References**

622 Abdalati, W. and Steffen, K.: Greenland Ice Sheet melt extent:1979-1999, J. Geophys. Res.  
623 Atmos., 106(D24), 33983–33988, doi:10.1029/2001JD900181, 2001.

624 Akagi, S. K., Yokelson, R. J., Wiedinmyer, C., Alvarado, M. J., Reid, J. S., Karl, T., Crouse, J.  
625 D. and Wennberg, P. O.: Emission factors for open and domestic biomass burning for use  
626 in atmospheric models, Atmos. Chem. Phys., 11(9), 4039–4072, doi:10.5194/acp-11-  
627 4039-2011, 2011.

628 AMAP: Snow, Water, Ice and Permafrost. Summary for Policy-makers, Arctic Monitoring  
629 and Assessment Programme (AMAP), Oslo, Norway. [online] Available from:  
630 [https://www.amap.no/documents/doc/Snow-Water-Ice-and-Permafrost-Summary-](https://www.amap.no/documents/doc/Snow-Water-Ice-and-Permafrost-Summary-for-Policy-makers/1532)  
631 [for-Policy-makers/1532](https://www.amap.no/documents/doc/Snow-Water-Ice-and-Permafrost-Summary-for-Policy-makers/1532) (Accessed 27 November 2017), 2017.

632 Anderson, C. H., Dibb, J. E., Griffin, R. J., Hagler, G. S. W. and Bergin, M. H.: Atmospheric  
633 water-soluble organic carbon measurements at Summit, Greenland, Atmos. Environ.,

634 42(22), 5612–5621, doi:10.1016/j.atmosenv.2008.03.006, 2008.

635 Andreae, M. O. and Gelencsér, A.: Black carbon or brown carbon? The nature of light-

636 absorbing carbonaceous aerosols, *Atmos. Chem. Phys.*, 6(3), 3419–3463,

637 doi:10.5194/acpd-6-3419-2006, 2006.

638 Antony, R., Mahalinganathan, K., Thamban, M. and Nair, S.: Organic carbon in antarctic

639 snow: Spatial trends and possible sources, *Environ. Sci. Technol.*, 45(23), 9944–9950,

640 doi:10.1021/es203512t, 2011.

641 Aurell, J. and Gullett, B. K.: Emission factors from aerial and ground measurements of

642 field and laboratory forest burns in the southeastern U.S.: PM<sub>2.5</sub>, black and brown

643 carbon, VOC, and PCDD/PCDF, *Environ. Sci. Technol.*, 47(15), 8443–8452,

644 doi:10.1021/es402101k, 2013.

645 BBC News: “Unusual” Greenland wildfires linked to peat, [online] Available from:

646 <http://www.bbc.com/news/science-environment-40877099> (Accessed 6 September

647 2017), 2017.

648 Bellouin, N. and Haywood, J.: *Aerosols: Climatology of Tropospheric Aerosols*, Second

649 Edi., Elsevier., 2014.

650 Benschoter, B. W. and Wieder, R. K.: Variability in organic matter lost by combustion in a

651 boreal bog during the 2001 Chisholm fire, *Can. J. For. Res.*, 33(12), 2509–2513,

652 doi:10.1139/x03-162, 2003.

653 Bond, T. C.: Spectral dependence of visible light absorption by carbonaceous particles

654 emitted from coal combustion, *Geophys. Res. Lett.*, 21(21), 4075–4078,

655 doi:10.1029/2001GL013652, 2001.

656 Bond, T. C., Doherty, S. J., Fahey, D. W., Forster, P. M., Berntsen, T., Deangelo, B. J., Flanner,

657 M. G., Ghan, S., Kärcher, B., Koch, D., Kinne, S., Kondo, Y., Quinn, P. K., Sarofim, M. C.,

658 Schultz, M. G., Schulz, M., Venkataraman, C., Zhang, H., Zhang, S., Bellouin, N., Guttikunda,

659 S. K., Hopke, P. K., Jacobson, M. Z., Kaiser, J. W., Klimont, Z., Lohmann, U., Schwarz, J. P.,

660 Shindell, D., Storelvmo, T., Warren, S. G. and Zender, C. S.: Bounding the role of black

661 carbon in the climate system: A scientific assessment, *J. Geophys. Res. Atmos.*, 118(11),

662 5380–5552, doi:10.1002/jgrd.50171, 2013.

663 Buras, R., Dowling, T. and Emde, C.: New secondary-scattering correction in DISORT with

664 increased efficiency for forward scattering, *J. Quant. Spectrosc. Radiat. Transf.*, 112(12),

665 2028–2034, doi:10.1016/j.jqsrt.2011.03.019, 2011.

666 Chakrabarty, R. K., Moosmüller, H., Chen, L. W. A., Lewis, K., Arnott, W. P., Mazzoleni, C.,

667 Dubey, M. K., Wold, C. E., Hao, W. M. and Kreidenweis, S. M.: Brown carbon in tar balls

668 from smoldering biomass combustion, *Atmos. Chem. Phys.*, 10(13), 6363–6370,

669 doi:10.5194/acp-10-6363-2010, 2010.

670 Chavez, P. S.: An improved dark-object subtraction technique for atmospheric scattering

671 correction of multispectral data, *Remote Sens. Environ.*, 24(3), 459–479,

672 doi:10.1016/0034-4257(88)90019-3, 1988.

673 Cofer III, W. R., Levine, J. S., Winstead, E. L. and Stocks, B. J.: New estimates of nitrous

674 oxide emissions from biomass burning, *Nature*, 349(6311), 689–691 [online] Available

675 from: <http://dx.doi.org/10.1038/349689a0>, 1991.

676 Conny, J. and Slater, J.: Black carbon and organic carbon in aerosol particles from crown

677 fires in the Canadian boreal forest, *J. Geophys. Res.* ... [online] Available from:

678 <http://onlinelibrary.wiley.com/doi/10.1029/2001JD001528/full>, 2002.

679 Daanen, R. P., Ingeman-Nielsen, T., Marchenko, S. S., Romanovsky, V. E., Foged, N.,

680 Stendel, M., Christensen, J. H. and Hornbech Svendsen, K.: Permafrost degradation risk

681 zone assessment using simulation models, *Cryosphere*, 5(4), 1043–1056,

682 doi:10.5194/tc-5-1043-2011, 2011.

683 Dahlback, A. and Stamnes, K.: A new spherical model for computing the radiation field  
684 available for photolysis and heating at twilight, *Planet. Space Sci.*, 39(5), 671–683,  
685 doi:10.1016/0032-0633(91)90061-E, 1991.

686 Davies, G. M., Gray, A., Rein, G. and Legg, C. J.: Peat consumption and carbon loss due to  
687 smouldering wildfire in a temperate peatland, *For. Ecol. Manage.*, 308, 169–177,  
688 doi:10.1016/j.foreco.2013.07.051, 2013.

689 Dibb, J. E., Arsenault, M., Peterson, M. C. and Honrath, R. E.: Fast nitrogen oxide  
690 photochemistry in Summit, Greenland snow, *Atmos. Environ.*, 36(15–16), 2501–2511,  
691 doi:10.1016/S1352-2310(02)00130-9, 2002.

692 Doherty, S. J., Warren, S. G., Grenfell, T. C., Clarke, A. D. and Brandt, R. E.: Light-absorbing  
693 impurities in Arctic snow, *Atmos. Chem. Phys.*, 10(23), 11647–11680, doi:10.5194/acp-  
694 10-11647-2010, 2010.

695 Drysdale, D.: *An Introduction to Fire Dynamics*, 3rd Editio., John Wiley & Sons, Ltd.,  
696 2011.

697 Emde, C., Buras-Schnell, R., Kylling, A., Mayer, B., Gasteiger, J., Hamann, U., Kylling, J.,  
698 Richter, B., Pause, C., Dowling, T. and Bugliaro, L.: The libRadtran software package for  
699 radiative transfer calculations (version 2.0.1), *Geosci. Model Dev.*, 9(5), 1647–1672,  
700 doi:10.5194/gmd-9-1647-2016, 2016.

701 Escuin, S., Navarro, R. and Fernández, P.: Fire severity assessment by using NBR  
702 (Normalized Burn Ratio) and NDVI (Normalized Difference Vegetation Index) derived  
703 from LANDSAT TM/ETM images, *Int. J. Remote Sens.*, 29(4), 1053–1073,  
704 doi:10.1080/01431160701281072, 2008.

705 Evangeliou, N., Balkanski, Y., Cozic, A., Hao, W. M. and Møller, A. P.: Wildfires in  
706 Chernobyl-contaminated forests and risks to the population and the environment: A  
707 new nuclear disaster about to happen?, *Environ. Int.*, 73, 346–358,  
708 doi:10.1016/j.envint.2014.08.012, 2014.

709 Evangeliou, N., Balkanski, Y., Cozic, A., Hao, W. M., Mouillot, F., Thonicke, K., Paugam, R.,  
710 Zibtsev, S., Mousseau, T. A., Wang, R., Poulter, B., Petkov, A., Yue, C., Cadule, P., Koffi, B.,  
711 Kaiser, J. W., Møller, A. P. and Classen, A. T.: Fire evolution in the radioactive forests of  
712 Ukraine and Belarus: Future risks for the population and the environment, *Ecol.*  
713 *Monogr.*, 85(1), 49–72, doi:10.1890/14-1227.1, 2015.

714 Evangeliou, N., Zibtsev, S., Myroniuk, V., Zhurba, M., Hamburger, T., Stohl, A., Balkanski,  
715 Y., Paugam, R., Mousseau, T. A., Møller, A. P. and Kireev, S. I.: Resuspension and  
716 atmospheric transport of radionuclides due to wildfires near the Chernobyl Nuclear  
717 Power Plant in 2015: An impact assessment., *Sci. Rep.*, 6, 26062 [online] Available from:  
718 <http://www.nature.com/srep/2016/160517/srep26062/full/srep26062.html>, 2016.

719 Fang, X., Thompson, R. L., Saito, T., Yokouchi, Y., Kim, J., Li, S., Kim, K. R., Park, S., Graziosi,  
720 F. and Stohl, A.: Sulfur hexafluoride (SF<sub>6</sub>) emissions in East Asia determined by inverse  
721 modeling, *Atmos. Chem. Phys.*, 14(9), 4779–4791, doi:10.5194/acp-14-4779-2014,  
722 2014.

723 Faulkner Burkhart, J., Kylling, A., Schaaf, C. B., Wang, Z., Bogren, W., Storvold, R., Solbø, S.,  
724 Pedersen, C. A. and Gerland, S.: Unmanned aerial system nadir reflectance and MODIS  
725 nadir BRDF-adjusted surface reflectances intercompared over Greenland, *Cryosphere*,  
726 11(4), 1575–1589, doi:10.5194/tc-11-1575-2017, 2017.

727 Feng, Y., Ramanathan, V. and Kotamarthi, V. R.: Brown carbon: A significant atmospheric  
728 absorber of solar radiation, *Atmos. Chem. Phys.*, 13(17), 8607–8621, doi:10.5194/acp-  
729 13-8607-2013, 2013.

730 Ferguson, S. A., Collins, R. L., Ruthford, J. and Fukuda, M.: Vertical distribution of  
731 nighttime smoke following a wildland biomass fire in boreal Alaska, *J. Geophys. Res.*,

732 108(June), D23, 4743, doi:10.1029/2002JD003324, doi:10.1029/2002JD003324, 2003.  
733 Fernandez Anez, N., Garcia Torrent, J., Medic Pejic, L. and Grima Olmedo, C.: Detection of  
734 incipient self-ignition process in solid fuels through gas emissions methodology, *J. Loss*  
735 *Prev. Process Ind.*, 36, 343–351, doi:10.1016/j.jlp.2015.02.010, 2015.  
736 Flanner, M. G., Zender, C. S., Randerson, J. T. and Rasch, P. J.: Present-day climate forcing  
737 and response from black carbon in snow, *J. Geophys. Res. Atmos.*, 112(11), 1–17,  
738 doi:10.1029/2006JD008003, 2007.  
739 Flanner, M. G., Zender, C. S., Hess, P. G., Mahowald, N. M., Painter, T. H., Ramanathan, V.  
740 and Rasch, P. J.: Springtime warming and reduced snow cover from carbonaceous  
741 particles, *Atmos. Chem. Phys.*, 9, 2481–2497, doi:10.5194/acp-9-2481-2009, 2009.  
742 Forster, C., Wandinger, U., Wotawa, G., James, P., Mattis, I., Althausen, D., Simmonds, P.,  
743 O’Doherty, S., Jennings, S. G., Kleefeld, C., Schneider, J., Trickl, T., Kreipl, S., Jäger, H. and  
744 Stohl, A.: Transport of boreal forest fire emissions from Canada to Europe, *J. Geophys.*  
745 *Res.*, 106, 22887, doi:10.1029/2001JD900115, 2001.  
746 Forster, C., Stohl, A. and Seibert, P.: Parameterization of convective transport in a  
747 Lagrangian particle dispersion model and its evaluation, *J. Appl. Meteorol. Climatol.*,  
748 46(4), 403–422, doi:10.1175/JAM2470.1, 2007.  
749 Freitas, S. R., Longo, K. M., Chatfield, R., Latham, D., Silva Dias, M. a. F., Andreae, M. O.,  
750 Prins, E., Santos, J. C., Gielow, R. and Carvalho, J. a.: Including the sub-grid scale plume  
751 rise of vegetation fires in low resolution atmospheric transport models, *Atmos. Chem.*  
752 *Phys. Discuss.*, 6(6), 11521–11559, doi:10.5194/acpd-6-11521-2006, 2006.  
753 Freitas, S. R., Longo, K. M., Trentmann, J. and Latham, D.: Technical Note: Sensitivity of 1-  
754 D smoke plume rise models to the inclusion of environmental wind drag, *Atmos. Chem.*  
755 *Phys.*, 10(2), 585–594, doi:10.5194/acp-10-585-2010, 2010.  
756 French, N., Kasischke, E., Hall, R., Murphy, K., Verbyla, D., Hoy, E. and Allen, J.: Using  
757 Landsat data to assess fire and burn severity in the North American boreal forest region:  
758 an overview and summary of results, *Int. J. Wildl. Fire*, 17(4), 443–462,  
759 doi:10.1071/WF08007, 2008.  
760 Fromm, M., Bevilacqua, R., Servranckx, R., Rosen, J., Thayer, J. P., Herman, J. and Larko, D.:  
761 Pyro-cumulonimbus injection of smoke to the stratosphere: Observations and impact of  
762 a super blowup in northwestern Canada on 3-4 August 1998, *J. Geophys. Res. D Atmos.*,  
763 110(8), 1–17, doi:10.1029/2004JD005350, 2005.  
764 Giglio, L., Descloitres, J., Justice, C. O. and Kaufman, Y. J.: An enhanced contextual fire  
765 detection algorithm for MODIS, *Remote Sens. Environ.*, 87(2–3), 273–282,  
766 doi:10.1016/S0034-4257(03)00184-6, 2003.  
767 Grannas, A. M., Shepson, P. B. and Filley, T. R.: Photochemistry and nature of organic  
768 matter in Arctic and Antarctic snow, *Global Biogeochem. Cycles*, 18(1), n/a-n/a,  
769 doi:10.1029/2003GB002133, 2004.  
770 Grythe, H., Kristiansen, N. I., Groot Zwaafink, C. D., Eckhardt, S., Ström, J., Tunved, P.,  
771 Krejci, R. and Stohl, A.: A new aerosol wet removal scheme for the Lagrangian particle  
772 model FLEXPARTv10, *Geosci. Model Dev.*, 10, 1447–1466, doi:10.5194/gmd-10-1447-  
773 2017, 2017.  
774 Hansen, J. and Nazarenko, L.: Soot climate forcing via snow and ice albedos, *Proc. Natl.*  
775 *Acad. Sci. U. S. A.*, 101(2), 423–428, doi:10.1073/pnas.2237157100, 2004.  
776 Hansen, J., Sato, M., Ruedy, R., Nazarenko, L., Lacis, A., Schmidt, G. A., Russell, G., Aleinov,  
777 I., Bauer, M., Bauer, S., Bell, N., Cairns, B., Canuto, V., Chandler, M., Cheng, Y., Del Genio, A.,  
778 Faluvegi, G., Fleming, E., Friend, A., Hall, T., Jackman, C., Kelley, M., Kiang, N., Koch, D.,  
779 Lean, J., Lerner, J., Lo, K., Menon, S., Miller, R., Minnis, P., Novakov, T., Oinas, V., Perlwitz,  
780 J., Perlwitz, J., Rind, D., Romanou, A., Shindell, D., Stone, P., Sun, S., Tausnev, N., Thresher,

781 D., Wielicki, B., Wong, T., Yao, M. and Zhang, S.: Efficacy of climate forcings, *J. Geophys.*  
782 *Res. D Atmos.*, 110(18), 1–45, doi:10.1029/2005JD005776, 2005.

783 Hao, W. M. and Ward, D. E.: Methane production from global biomass burning, *J.*  
784 *Geophys. Res. Atmos.*, 98(D11), 20657–20661, doi:10.1029/93JD01908, 1993.

785 Hao, W. M., Petkov, A., Nordgren, B. L., Silverstein, R. P., Corley, R. E., Urbanski, S. P.,  
786 Evangeliou, N., Balkanski, Y. and Kinder, B.: Daily black carbon emissions from fires in  
787 Northern Eurasia from 2002 to 2013, *Geosci. Model Dev.*, 9, 4461–4474,  
788 doi:10.5194/gmd-9-4461-2016, 2016.

789 Holben, B. N.: Characteristics of maximum-value composite images from temporal  
790 AVHRR data, *Int. J. Remote Sens.*, 7(11), 1417–1434, doi:10.1080/01431168608948945,  
791 1986.

792 Holben, B. N., Eck, T. F., Slutsker, I., Tanré, D., Buis, J. P., Setzer, A., Vermote, E., Reagan, J.  
793 A., Kaufman, Y. J., Nakajima, T., Lavenu, F., Jankowiak, I. and Smirnov, A.: AERONET—A  
794 Federated Instrument Network and Data Archive for Aerosol Characterization, *Remote*  
795 *Sens. Environ.*, 66(1), 1–16, doi:10.1016/S0034-4257(98)00031-5, 1998.

796 Hosseini, S., Li, Q., Cocker, D., Weise, D., Miller, A., Shrivastava, M., Miller, J. W.,  
797 Mahalingam, S., Princevac, M. and Jung, H.: Particle size distributions from laboratory-  
798 scale biomass fires using fast response instruments, *Atmos. Chem. Phys.*, 10(16), 8065–  
799 8076, doi:10.5194/acp-10-8065-2010, 2010.

800 Hu, Y., Fernandez-Anez, N., Smith, T. E. L. and Rein, G.: Review of emissions from  
801 smouldering peat fires and their contribution to regional haze episodes, *Int. J. Wildl.*  
802 *Fire*, 27(5), 293–312, doi:10.1071/WF17084, 2018.

803 IPCC: Climate Change 2013: The Physical Science Basis. Contribution to the Fifth  
804 Assessment Report of the Intergovernmental Panel on Climate Change., edited by T. F.  
805 Stocker, D. Qin, G.-K. Plattner, M. M. B. Tignor, S. K. Allen, J. Boschung, A. Nauels, Y. Xia, V.  
806 Bex, and P. M. Midgley, Cambridge University Press., 2013.

807 Jacobson, M. Z.: Strong radiative heating due to the mixing state of black carbon in  
808 atmospheric aerosols, *Nature*, 409(6821), 695–697, doi:10.1038/35055518, 2001.

809 Jedrzejek, B., Drees, B., Daniëls, F. J. A. and Hölzel, N.: Vegetation pattern of mountains in  
810 West Greenland - a baseline for long-term surveillance of global warming impacts, *Plant*  
811 *Ecol. Divers.*, 6(3–4), 405–422, doi:10.1080/17550874.2013.802049, 2013.

812 Jo, D. S., Park, R. J., Lee, S., Kim, S. W. and Zhang, X.: A global simulation of brown carbon:  
813 Implications for photochemistry and direct radiative effect, *Atmos. Chem. Phys.*, 16(5),  
814 3413–3432, doi:10.5194/acp-16-3413-2016, 2016.

815 Justice, C. O., Giglio, L., Korontzi, S., Owens, J., Morisette, J. T., Roy, D., Descloitres, J.,  
816 Alleaume, S., Petitcolin, F. and Kaufman, Y.: The MODIS fire products, *Remote Sens.*  
817 *Environ.*, 83(1–2), 244–262, doi:10.1016/S0034-4257(02)00076-7, 2002.

818 Kaiser, J. W., Heil, A., Andreae, M. O., Benedetti, A., Chubarova, N., Jones, L., Morcrette, J. J.,  
819 Razinger, M., Schultz, M. G., Suttie, M. and Van Der Werf, G. R.: Biomass burning  
820 emissions estimated with a global fire assimilation system based on observed fire  
821 radiative power, *Biogeosciences*, 9(1), 527–554, doi:10.5194/bg-9-527-2012, 2012.

822 Kato, S., Ackerman, T. P., Mather, J. H. and Clothiaux, E. E.: The k-distribution method and  
823 correlated-k approximation for a shortwave radiative transfer model, *J. Quant.*  
824 *Spectrosc. Radiat. Transf.*, 62(1), 109–121, doi:10.1016/S0022-4073(98)00075-2, 1999.

825 Keegan, K. M., Albert, M. R., McConnell, J. R. and Baker, I.: Climate change and forest fires  
826 synergistically drive widespread melt events of the Greenland Ice Sheet, , 1–4,  
827 doi:10.1073/pnas.1405397111, 2014.

828 Key, C. H. and Benson, N. C.: Landscape assessment: Sampling and analysis methods,  
829 USDA For. Serv. Gen. Tech. Rep. RMRS-GTR-164-CD, (June), 1–55,



830 doi:10.1002/app.1994.070541203, 2006.

831 Klimont, Z., Kupiainen, K., Heyes, C., Purohit, P., Cofala, J., Rafaj, P., Borken-Kleefeld, J. and  
832 Schöpp, W.: Global anthropogenic emissions of particulate matter including black  
833 carbon, *Atmos. Chem. Phys.*, 17, 8681–8723, doi:10.5194/acp-17-508681-2017, 2017.

834 Lavoie, C. and Pellerin, S.: Fires in temperate peatlands (southern Quebec): past and  
835 recent trends, *Can. J. Bot.*, 85(3), 263–272, doi:10.1139/B07-012, 2007.

836 Legrand, M., Preunkert, S., Jourdain, B., Guilhermet, J., Faïn, X., Alekhina, I. and Petit, J. R.:  
837 Water-soluble organic carbon in snow and ice deposited at Alpine, Greenland, and  
838 Antarctic sites: A critical review of available data and their atmospheric relevance, *Clim.  
839 Past*, 9(5), 2195–2211, doi:10.5194/cp-9-2195-2013, 2013.

840 Legrand, M., McConnell, J., Fischer, H., Wolff, E. W., Preunkert, S., Arienzo, M., Chellman,  
841 N., Leuenberger, D., Maselli, O., Place, P., Sigl, M., Schizpbach, S. and Flannigan, M.:  
842 Boreal fire records in Northern Hemisphere ice cores: A review, *Clim. Past*, 12(10),  
843 2033–2059, doi:10.5194/cp-12-2033-2016, 2016.

844 Leino, K., Riuttanen, L., Nieminen, T., Väänänen, R., Pohja, T., Keronen, P., Järvi, L., Aalto,  
845 P. P., Virkkula, A., Kerminen, V. M., Petäjä, T., Kulmala, M., Nieminen, T., Dal Maso, M. and  
846 Virkkula, A.: Biomass-burning smoke episodes in Finland from eastern European  
847 wildfires, *Boreal Environ. Res.*, 19(x), 275–292, 2014.

848 Lelieveld, J., Evans, J. S., Fnais, M., Giannadaki, D. and Pozzer, A.: The contribution of  
849 outdoor air pollution sources to premature mortality on a global scale., *Nature*,  
850 525(7569), 367–71, doi:10.1038/nature15371, 2015.

851 Leung, F. Y. T., Logan, J. A., Park, R., Hyer, E., Kasischke, E., Streets, D. and Yurganov, L.:  
852 Impacts of enhanced biomass burning in the boreal forests in 1998 on tropospheric  
853 chemistry and the sensitivity of model results to the injection height of emissions, *J.  
854 Geophys. Res. Atmos.*, 112(10), 1–15, doi:10.1029/2006JD008132, 2007.

855 Lim, H. J., Turpin, B. J., Russell, L. M. and Bates, T. S.: Organic and elemental carbon  
856 measurements during ACE-Asia suggest a longer atmospheric lifetime for elemental  
857 carbon, *Environ. Sci. Technol.*, 37(14), 3055–3061, doi:10.1021/es020988s, 2003.

858 Limbeck, A., Kulmala, M. and Puxbaum, H.: Secondary organic aerosol formation in the  
859 atmosphere via heterogeneous reaction of gaseous isoprene on acidic particles,  
860 *Geophys. Res. Lett.*, 30(19), 4–7, doi:10.1029/2003GL017738, 2003.

861 Long, C. M., Nascarella, M. A. and Valberg, P. A.: Carbon black vs. black carbon and other  
862 airborne materials containing elemental carbon: Physical and chemical distinctions,  
863 *Environ. Pollut.*, 181, 271–286, doi:10.1016/j.envpol.2013.06.009, 2013.

864 Lyons, W. B., Welch, K. A. and Doggett, J. K.: Organic carbon in Antarctic snow, *Geophys.  
865 Res. Lett.*, 34(2), 2–5, doi:10.1029/2006GL028150, 2007.

866 Magnan, G., Lavoie, M. and Payette, S.: Impact of fire on long-term vegetation dynamics  
867 of ombrotrophic peatlands in northwestern Québec, Canada, *Quat. Res.*, 77(1), 110–121,  
868 doi:http://dx.doi.org/10.1016/j.yqres.2011.10.006, 2012.

869 Massling, A., Nielsen, I. E., Kristensen, D., Christensen, J. H., Sorensen, L. L., Jensen, B.,  
870 Nguyen, Q. T., Nøjgaard, J. K., Glasius, M. and Skov, H.: Atmospheric black carbon and  
871 sulfate concentrations in Northeast Greenland, *Atmos. Chem. Phys.*, 15(16), 9681–9692,  
872 doi:10.5194/acp-15-9681-2015, 2015.

873 Mayer, B. and Kylling, A.: Technical note: The libRadtran software package for radiative  
874 transfer calculations - description and examples of use, *Atmos. Chem. Phys.*, 5(7), 1855–  
875 1877, doi:10.5194/acp-5-1855-2005, 2005.

876 Mukai, H. and Ambe, Y.: Characterization of a humic acid-like brown substance in  
877 airborne particulate matter and tentative identification of its origin, *Atmos. Environ.*,  
878 20(5), 813–819, doi:https://doi.org/10.1016/0004-6981(86)90265-9, 1986.

879 Myhre, G., Shindell, D., Bréon, F.-M., Collins, W., Fuglestedt, J., Huang, J., Koch, D.,  
880 Lamarque, J.-F., Lee, D., Mendoza, B., Nakajima, T., Robock, A., Stephens, G., Takemura, T.  
881 and Zhang, H.: Anthropogenic and Natural Radiative Forcing, in *Climate Change 2013:*  
882 *The Physical Science Basis. Contribution of Working Group I to the Fifth Assessment*  
883 *Report of the Intergovernmental Panel on Climate Change*, edited by Stocker, T.F., D. Qin,  
884 G.-K. Plattner, M. Tignor, S. K. Allen, J. Boschung, A. Nauels, Y. Xia, V. Bex, and P. M.  
885 Midgley, pp. 659–740, Cambridge University Press, Cambridge, United Kingdom and  
886 New York, NY, USA., 2013.

887 NASA: FIRMS. Web Fire Mapper, [online] Available from:  
888 <https://firms.modaps.eosdis.nasa.gov/firemap/> (Accessed 5 September 2017a), 2017.

889 NASA: Roundtable: The Greenland Wildfire, [online] Available from:  
890 [https://earthobservatory.nasa.gov/blogs/earthmatters/2017/08/10/roundtable-the-](https://earthobservatory.nasa.gov/blogs/earthmatters/2017/08/10/roundtable-the-greenland-wildfire/)  
891 [greenland-wildfire/](https://earthobservatory.nasa.gov/blogs/earthmatters/2017/08/10/roundtable-the-greenland-wildfire/) (Accessed 6 September 2017b), 2017.

892 NASA: Wildfires Continue to Beleaguer Western Canada, [online] Available from:  
893 [https://www.nasa.gov/image-feature/goddard/2017/wildfires-continue-to-beleaguer-](https://www.nasa.gov/image-feature/goddard/2017/wildfires-continue-to-beleaguer-western-canada)  
894 [western-canada](https://www.nasa.gov/image-feature/goddard/2017/wildfires-continue-to-beleaguer-western-canada) (Accessed 29 October 2017c), 2017.

895 New Scientist Magazine: Largest ever wildfire in Greenland seen burning from space,  
896 [online] Available from: [https://www.newscientist.com/article/2143159-largest-ever-](https://www.newscientist.com/article/2143159-largest-ever-wildfire-in-greenland-seen-burning-from-space/)  
897 [wildfire-in-greenland-seen-burning-from-space/](https://www.newscientist.com/article/2143159-largest-ever-wildfire-in-greenland-seen-burning-from-space/) (Accessed 6 September 2017), 2017.

898 Page, S. E., Siegert, F., Rieley, J. O., Boehm, H.-D. V., Jada, A. and Limin, S.: The amount of  
899 carbon released from peat and forest fires in Indonesia during 1997, *Nature*, 420(19),  
900 61–65, doi:10.1038/nature01131, 2015.

901 Paugam, R., Wooster, M. and Atherton, J.: Development and optimization of a wildfire  
902 plume rise model based on remote sensing data inputs – Part 2, , doi:10.5194/acpd-15-  
903 9815-2015, 2015.

904 Pokhrel, R. P., Wagner, N. L., Langridge, J. M., Lack, D. A., Jayarathne, T., Stone, E. A.,  
905 Stockwell, C. E., Yokelson, R. J. and Murphy, S. M.: Parameterization of single-scattering  
906 albedo (SSA) and absorption Ångström exponent (AAE) with EC/OC for aerosol  
907 emissions from biomass burning, *Atmos. Chem. Phys.*, 16(15), 9549–9561,  
908 doi:10.5194/acp-16-9549-2016, 2016.

909 Polashenski, C. M., Dibb, J. E., Flanner, M. G., Chen, J. Y., Courville, Z. R., Lai, A. M., Schauer,  
910 J. J., Shafer, M. M. and Bergin, M.: Neither dust nor black carbon causing apparent albedo  
911 decline in Greenland’s dry snow zone: Implications for MODIS C5 surface reflectance,  
912 *Geophys. Res. Lett.*, 42(21), 9319–9327, doi:10.1002/2015GL065912, 2015.

913 Randerson, J. T., Chen, Y., Van Der Werf, G. R., Rogers, B. M. and Morton, D. C.: Global  
914 burned area and biomass burning emissions from small fires, *J. Geophys. Res.*  
915 *Biogeosciences*, 117(4), doi:10.1029/2012JG002128, 2012.

916 Reddy, A. D., Hawbaker, T. J., Wurster, F., Zhu, Z., Ward, S., Newcomb, D. and Murray, R.:  
917 Quantifying soil carbon loss and uncertainty from a peatland wildfire using multi-  
918 temporal LiDAR, *Remote Sens. Environ.*, 170, 306–316, doi:10.1016/j.rse.2015.09.017,  
919 2015.

920 Rémy, S., Veira, A., Paugam, R., Sofiev, M., Kaiser, J. W., Marengo, F., Burton, S. P.,  
921 Benedetti, A., Engelen, R. J., Ferrare, R. and Hair, J. W.: Two global data sets of daily fire  
922 emission injection heights since 2003, , 2921–2942, doi:10.5194/acp-17-2921-2017,  
923 2017.

924 Restuccia, F., Ptak, N. and Rein, G.: Self-heating behavior and ignition of shale rock,  
925 *Combust. Flame*, 176, 213–219, doi:10.1016/j.combustflame.2016.09.025, 2017a.

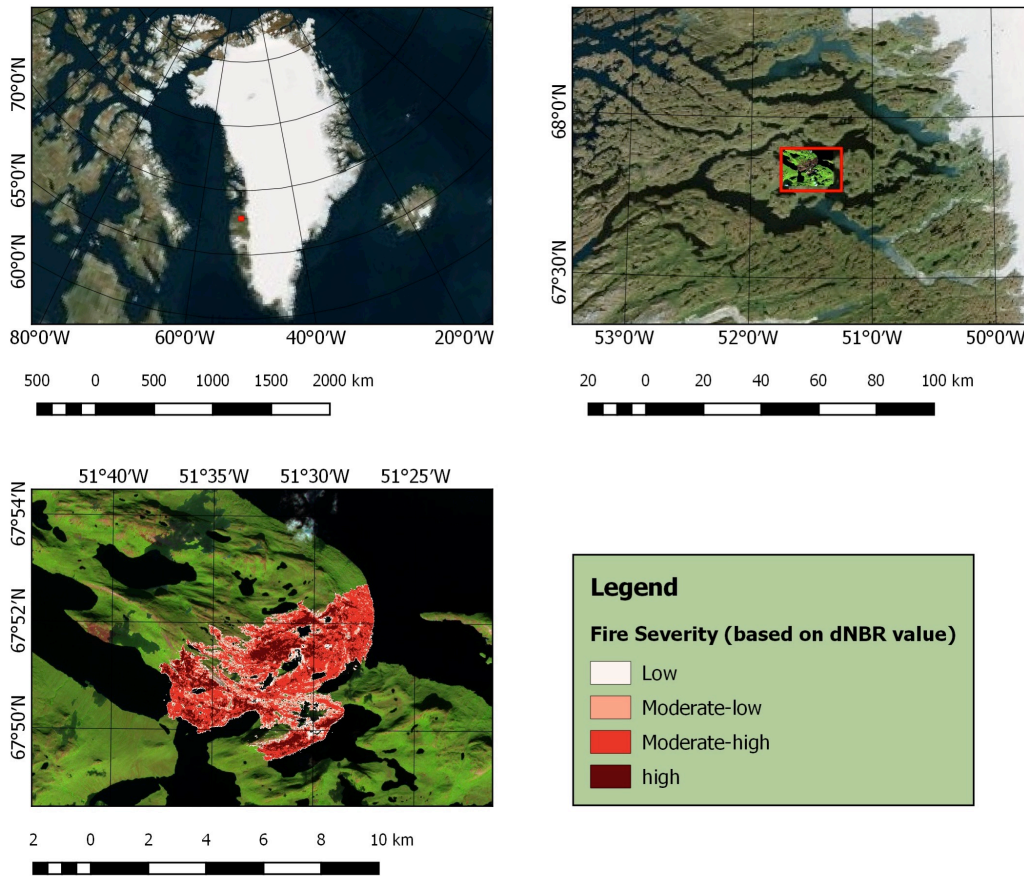
926 Restuccia, F., Huang, X. and Rein, G.: Self-ignition of natural fuels: Can wildfires of  
927 carbon-rich soil start by self-heating?, *Fire Saf. J.*, 91(February), 828–834,

928 doi:10.1016/j.firesaf.2017.03.052, 2017b.  
929 von Schneidemesser, E., Schauer, J. J., Hagler, G. S. W. and Bergin, M. H.: Concentrations  
930 and sources of carbonaceous aerosol in the atmosphere of Summit, Greenland, *Atmos.*  
931 *Environ.*, 43(27), 4155–4162, doi:10.1016/j.atmosenv.2009.05.043, 2009.  
932 Seiler, W. and Crutzen, P. J.: Estimates of gross and net fluxes of carbon between the  
933 biosphere and the atmosphere from biomass burning, *Clim. Change*, 2(3), 207–247,  
934 doi:10.1007/BF00137988, 1980.  
935 SERMITSIAQ: Se billeder: Naturbrand udvikler kraftig røg, , in Danish [online] Available  
936 from: <http://sermitsiaq.ag/se-billeder-naturbrand-udvikler-kraftig-roeg> (Accessed 6  
937 September 2017), 2017.  
938 Shetler, G., Turetsky, M. R., Kane, E. and Kasischke, E.: Sphagnum mosses limit total  
939 carbon consumption during fire in Alaskan black spruce forests, *Can. J. For. Res.*, 38(8),  
940 2328–2336, doi:10.1139/X08-057, 2008.  
941 Shi, Y., Matsunaga, T., Saito, M., Yamaguchi, Y. and Chen, X.: Comparison of global  
942 inventories of CO<sub>2</sub> emissions from biomass burning during 2002–2011 derived from  
943 multiple satellite products, *Environ. Pollut.*, 206, 479–487,  
944 doi:10.1016/j.envpol.2015.08.009, 2015.  
945 Skeie, R. B., Berntsen, T., Myhre, G., Pedersen, C. A., Ström, J., Gerland, S. and Ogren, J. A.:  
946 Black carbon in the atmosphere and snow, from pre-industrial times until present,  
947 *Atmos. Chem. Phys.*, 11(14), 6809–6836, doi:10.5194/acp-11-6809-2011, 2011.  
948 Smirnov, N. S., Korotkov, V. N. and Romanovskaya, A. A.: Black carbon emissions from  
949 wildfires on forest lands of the Russian Federation in 2007–2012, *Russ. Meteorol.*  
950 *Hydrol.*, 40(7), 435–442, doi:10.3103/S1068373915070018, 2015.  
951 Stamnes, K., Tsay, S.-C., Wiscombe, W. and Jayaweera, K.: Numerically stable algorithm  
952 for discrete-ordinate-method radiative transfer in multiple scattering and emitting  
953 layered media, *Appl. Opt.*, 27(12), 2502, doi:10.1364/AO.27.002502, 1988.  
954 Stendel, M., Christensen, J. H. and Petersen, D.: Arctic Climate and Climate Change with a  
955 Focus on Greenland, *Adv. Ecol. Res.*, 40(07), 13–43, doi:10.1016/S0065-  
956 2504(07)00002-5, 2008.  
957 Stockwell, C. E., Jayarathne, T., Cochrane, M. A., Ryan, K. C., Putra, E. I., Saharjo, B. H.,  
958 Nurhayati, A. D., Albar, I., Blake, D. R., Simpson, I. J., Stone, E. A. and Yokelson, R. J.: Field  
959 measurements of trace gases and aerosols emitted by peat fires in Central Kalimantan,  
960 Indonesia, during the 2015 El Niño, *Atmos. Chem. Phys.*, 16(18), 11711–11732,  
961 doi:10.5194/acp-16-11711-2016, 2016.  
962 Stohl, A., Forster, C., Frank, A., Seibert, P. and Wotawa, G.: Technical note: The Lagrangian  
963 particle dispersion model FLEXPART version 6.2, *Atmos. Chem. Phys.*, 5(9), 2461–2474,  
964 doi:10.5194/acp-5-2461-2005, 2005.  
965 Stohl, A., Andrews, E., Burkhart, J. F., Forster, C., Herber, A., Hoch, S. W., Kowal, D.,  
966 Lunder, C., Mefford, T., Ogren, J. A., Sharma, S., Spichtinger, N., Stebel, K., Stone, R., Ström,  
967 J., Tørseth, K., Wehrl, C. and Yttri, K. E.: Pan-Arctic enhancements of light absorbing  
968 aerosol concentrations due to North American boreal forest fires during summer 2004, *J.*  
969 *Geophys. Res. Atmos.*, 111(22), 1–20, doi:10.1029/2006JD007216, 2006.  
970 Stohl, A., Berg, T., Burkhart, J. F., Fjærraa, A. M., Forster, C., Herber, A., Hov, Ø., Lunder, C.,  
971 McMillan, W. W., Oltmans, S., Shiobara, M., Simpson, D., Solberg, S., Stebel, K., Ström, J.,  
972 Tørseth, K., Treffeisen, R., Virkkunen, K. and Yttri, K. E.: Arctic smoke &ndash; record  
973 high air pollution levels in the European Arctic due to agricultural fires in Eastern  
974 Europe in spring 2006, *Atmos. Chem. Phys.*, 7(2), 511–534, doi:10.5194/acp-7-511-  
975 2007, 2007.  
976 Stohl, A., Prata, A. J., Eckhardt, S., Clarisse, L., Durant, A., Henne, S., Kristiansen, N. I.,

977 Minikin, A., Schumann, U., Seibert, P., Stebel, K., Thomas, H. E., Thorsteinsson, T., Tørseth,  
978 K. and Weinzierl, B.: Determination of time-and height-resolved volcanic ash emissions  
979 and their use for quantitative ash dispersion modeling: The 2010 Eyjafjallajökull  
980 eruption, *Atmos. Chem. Phys.*, 11(9), 4333–4351, doi:10.5194/acp-11-4333-2011, 2011.  
981 Stohl, A., Klimont, Z., Eckhardt, S., Kupiainen, K., Shevchenko, V. P., Kopeikin, V. M. and  
982 Novigatsky, A. N.: Black carbon in the Arctic: The underestimated role of gas flaring and  
983 residential combustion emissions, *Atmos. Chem. Phys.*, 13(17), 8833–8855,  
984 doi:10.5194/acp-13-8833-2013, 2013.  
985 Stroeve, J., Box, J. E., Gao, F., Liang, S., Nolin, A. and Schaaf, C.: Accuracy assessment of the  
986 MODIS 16-day albedo product for snow: Comparisons with Greenland in situ  
987 measurements, *Remote Sens. Environ.*, 94(1), 46–60, doi:10.1016/j.rse.2004.09.001,  
988 2005.  
989 Sunderman, S. O. and Weisberg, P. J.: Remote sensing approaches for reconstructing fire  
990 perimeters and burn severity mosaics in desert spring ecosystems, *Remote Sens.*  
991 *Environ.*, 115(9), 2384–2389, doi:10.1016/j.rse.2011.05.001, 2011.  
992 Turetsky, M. R., Donahue, W. F. and Benscoter, B. W.: Experimental drying intensifies  
993 burning and carbon losses in a northern peatland, *Nat. Commun.*, 2, 514,  
994 doi:10.1038/ncomms1523, 2011.  
995 Turetsky, M. R., Benscoter, B., Page, S., Rein, G., van der Werf, G. R. and Watts, A.: Global  
996 vulnerability of peatlands to fire and carbon loss, *Nat. Geosci.*, 8(1), 11–14,  
997 doi:10.1038/ngeo2325, 2014.  
998 Urbanski, S. P., Hao, W. M. and Nordgren, B.: The wildland fire emission inventory:  
999 Western United States emission estimates and an evaluation of uncertainty, *Atmos.*  
1000 *Chem. Phys.*, 11(24), 12973–13000, doi:10.5194/acp-11-12973-2011, 2011.  
1001 Wandji Nyamsi, W., Arola, A., Blanc, P., Lindfors, a. V., Cesnulyte, V., Pitkänen, M. R. a. and  
1002 Wald, L.: Technical Note: A novel parameterization of the transmissivity due to ozone  
1003 absorption in the distribution method and correlated approximation of Kato et al.  
1004 (1999) over the UV band, *Atmos. Chem. Phys.*, 15(13), 7449–7456, doi:10.5194/acp-15-  
1005 7449-2015, 2015.  
1006 Warren, S. G.: Can black carbon in snow be detected by remote sensing?, *J. Geophys. Res.*  
1007 *Atmos.*, 118(2), 779–786, doi:10.1029/2012JD018476, 2013.  
1008 Wieder, R. K., Scott, K. D., Kamminga, K., Vile, M. A., Vitt, D. H., Bone, T., Xu, B., Benscoter,  
1009 B. W. and Bhatti, J. S.: Postfire carbon balance in boreal bogs of Alberta, Canada, *Glob.*  
1010 *Chang. Biol.*, 15(1), 63–81, doi:10.1111/j.1365-2486.2008.01756.x, 2009.  
1011 Winiger, P., Andersson, A., Eckhardt, S., Stohl, A., Semiletov, I. P., Dudarev, O. V., Charkin,  
1012 A., Shakhova, N., Klimont, Z., Heyes, C. and Gustafsson, Ö.: Siberian Arctic black carbon  
1013 sources constrained by model and observation, *Proc. Natl. Acad. Sci.*, 114(7), E1054–  
1014 E1061, doi:10.1073/pnas.1613401114, 2017.  
1015 Winker, D. M., Vaughan, M. A., Omar, A., Hu, Y., Powell, K. A., Liu, Z., Hunt, W. H. and  
1016 Young, S. A.: Overview of the CALIPSO mission and CALIOP data processing algorithms, *J.*  
1017 *Atmos. Ocean. Technol.*, 26(11), 2310–2323, doi:10.1175/2009JTECHA1281.1, 2009.  
1018 Wu, D., Huang, X., Norman, F., Verplaetsen, F., Berghmans, J. and Van Den Bulck, E.:  
1019 Experimental investigation on the self-ignition behaviour of coal dust accumulations in  
1020 oxy-fuel combustion system, *Fuel*, 160, 245–254, doi:10.1016/j.fuel.2015.07.050, 2015.  
1021 Wu, G. M., Cong, Z. Y., Kang, S. C., Kawamura, K., Fu, P. Q., Zhang, Y. L., Wan, X., Gao, S. P.  
1022 and Liu, B.: Brown carbon in the cryosphere: Current knowledge and perspective, *Adv.*  
1023 *Clim. Chang. Res.*, 7(1–2), 82–89, doi:10.1016/j.accre.2016.06.002, 2016.  
1024 Zhuravleva, T. B., Kabanov, D. M., Nasrtdinov, I. M., Russkova, T. V., Sakerin, S. M.,  
1025 Smirnov, A. and Holben, B. N.: Radiative characteristics of aerosol during extreme fire

1026 event over Siberia in summer 2012, Atmos. Meas. Tech., 10(1), 179–198,  
1027 doi:10.5194/amt-10-179-2017, 2017.  
1028  
1029

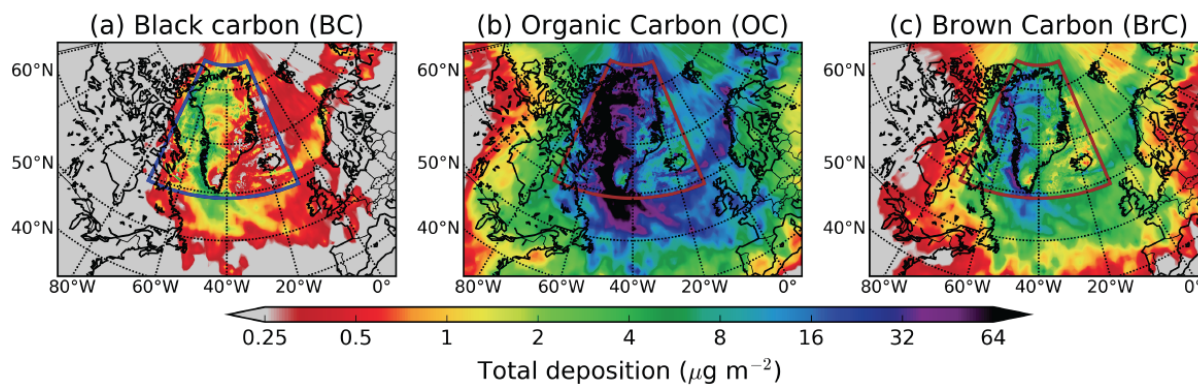
1030 **FIGURE LEGENDS**



1031 **Figure 1.** Map of Greenland (upper left) and zoomed map marked with fire location (upper  
1032 right and burned area classification (bottom) in terms of fire severity according to Sentinel 2A  
1033 images for fires burning in Greenland in August 2017. To delineate fire perimeters, both  
1034 Landsat 8 OLI and Sentinel 1A – 2A data were used (Table 1).  
1035

1036

## CUMULATIVE DEPOSITION (31 August 2017)

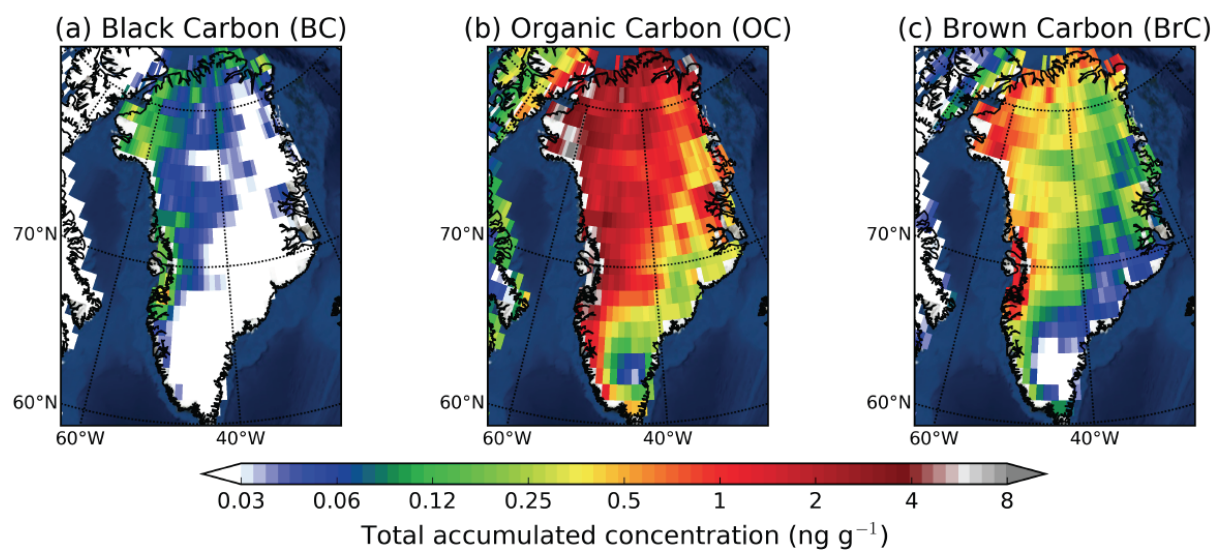


1037

1038 **Figure 2.** Total (wet and dry) deposition of (a) BC, (b) OC and (c) BrC (in  $\mu\text{g m}^{-2}$ ) from the  
1039 Greenland fires until 31 August 2017. The colored rectangle depicts the nested high-  
1040 resolution domain.

1041

### SNOW CONCENTRATIONS BASED ON SNOW ACCUMULATION FROM ECMWF



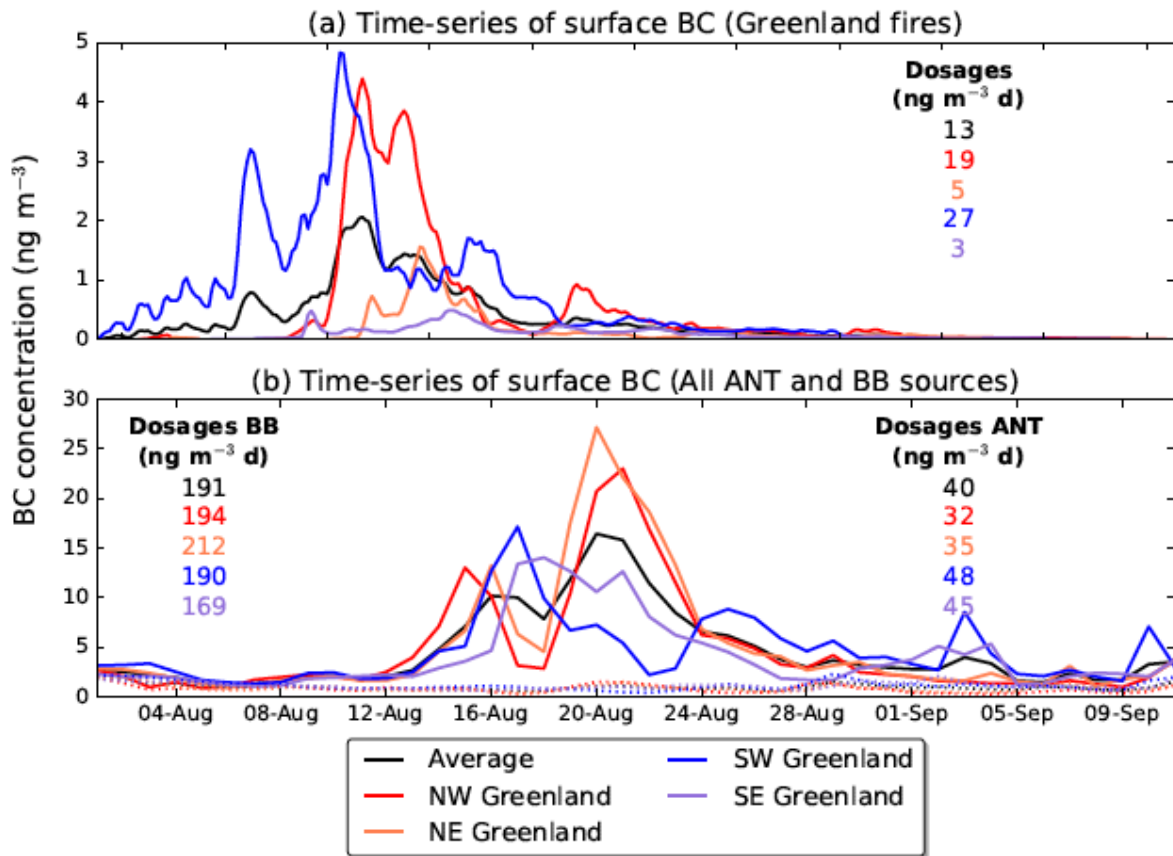
1042

1043 **Figure 3.** Calculated snow concentrations of (a) BC, (b) OC and (c) BrC over Greenland  
1044 based on the modeled deposition and the snow precipitation (large scale and convective)  
1045 adopted from the operational ECMWF data that were used in our simulation (see section 2.3).

1046



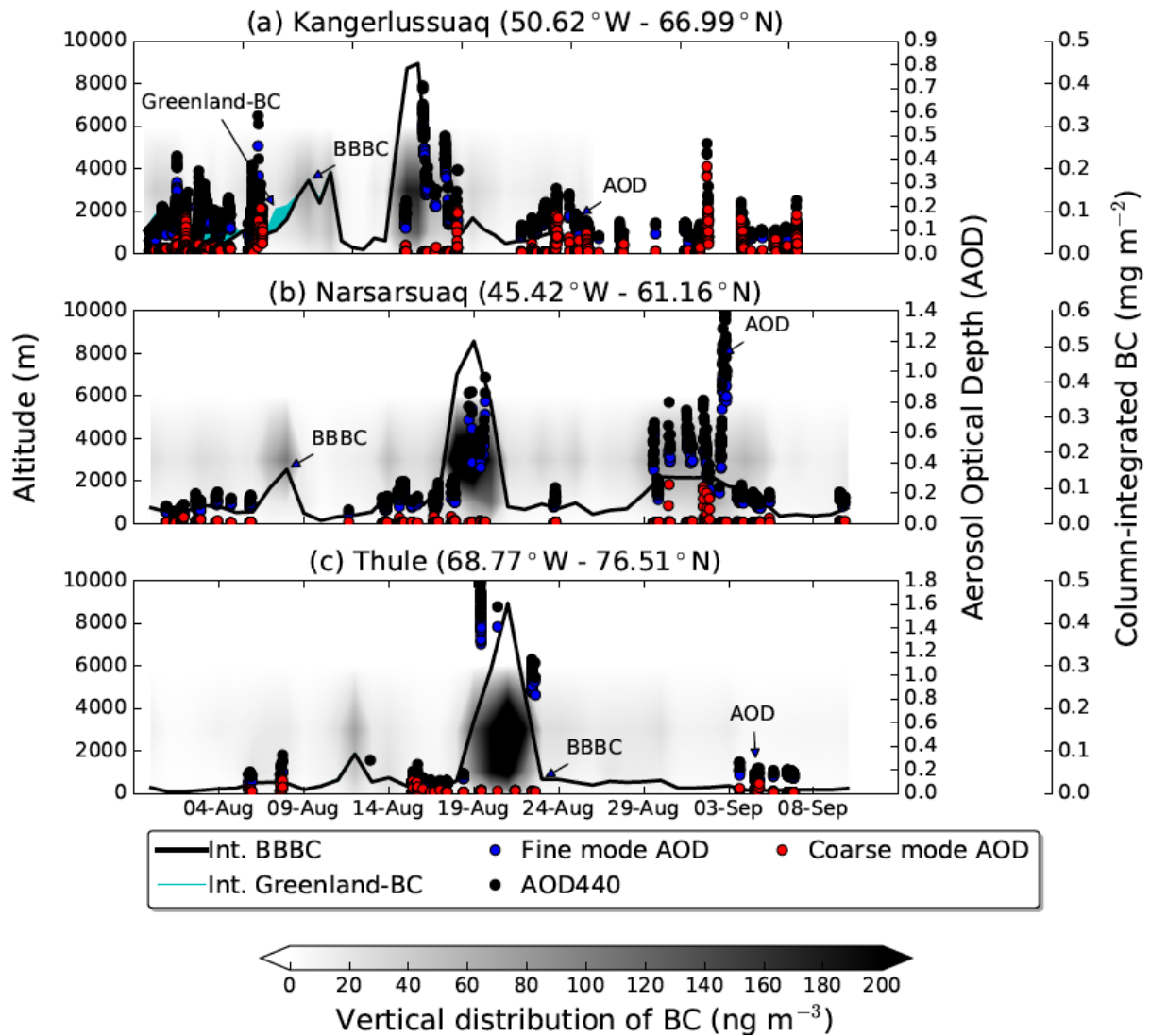
1047



1048

1049 **Figure 4.** (a) Time-series of surface BC concentrations in Northwestern, Northeastern,  
1050 Southwestern and Southeastern Greenland from the summer 2017 fires in Western Greenland.  
1051 (b) Time-series of surface BC concentrations in Northwestern, Northeastern, Southwestern  
1052 and Southeastern Greenland from global anthropogenic (ANT, dashed lines) and biomass  
1053 burning (BB, solid lines) emissions for the same period. The numbers represent the respective  
1054 dosages (time-integrated concentrations) for the time period shown. The color codes are  
1055 reported in the legend.

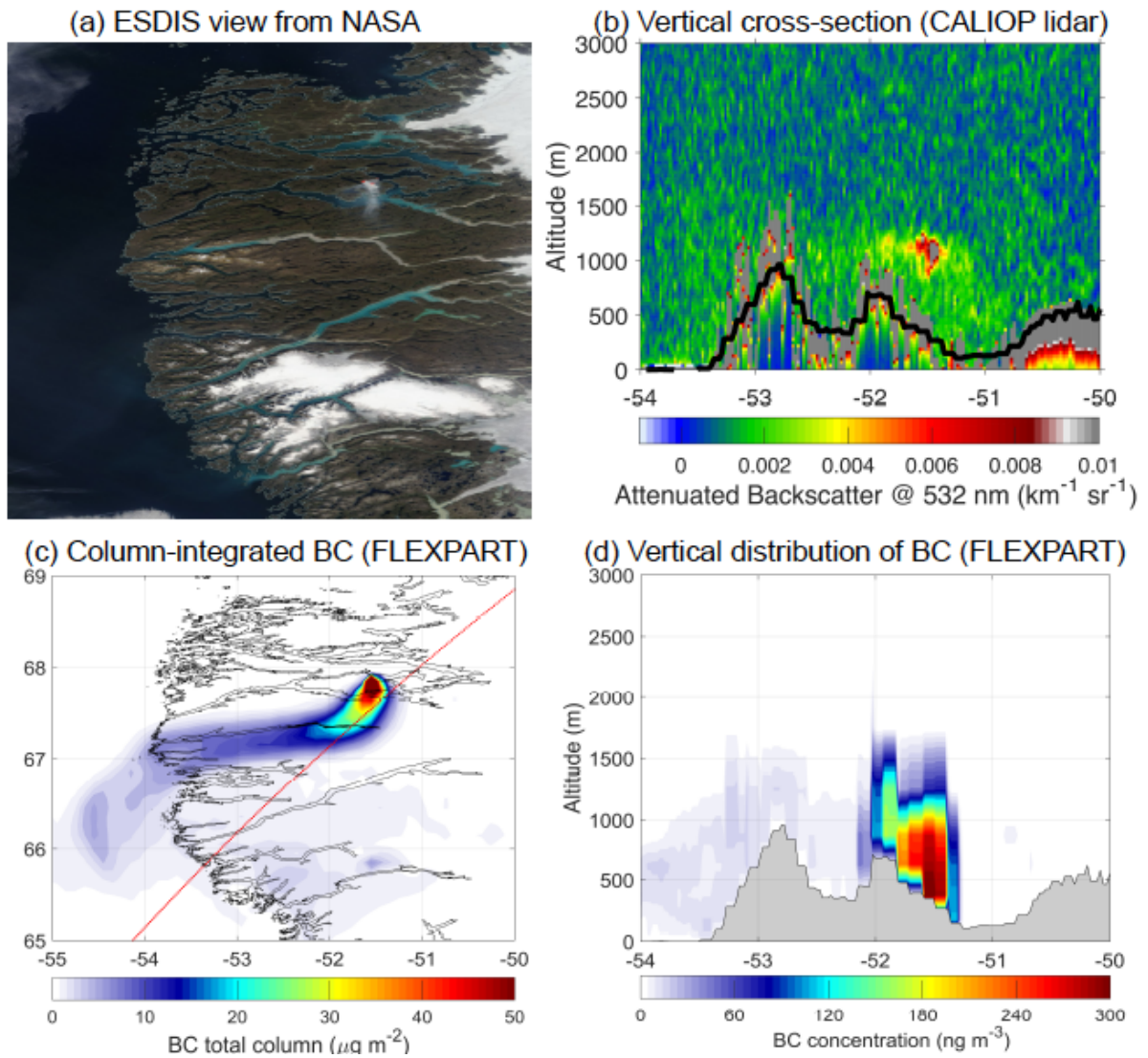
1056



1057

1058 **Figure 5.** Contour plot of the vertical distribution of simulated BC (altitude a.g.l. shown on  
 1059 left y-axis) as a function of time (x-axis) and time-series of column-integrated simulated BC  
 1060 (extended right axis) from fires burning outside Greenland (black line) and Greenland fires  
 1061 (cyan stacked area). Column-integrated BC from anthropogenic sources was extremely small  
 1062 and it is not plotted here. Time-series for fine mode (blue) and coarse (red) AOD at 500 nm  
 1063 and total AOD at 400 nm (black) correspond to the right y-axis. The three panels show results  
 1064 for stations (a) Kangerlussuaq, (b) Narsarsuaq and (c) Thule (sorted from the closest to the  
 1065 farthest station).

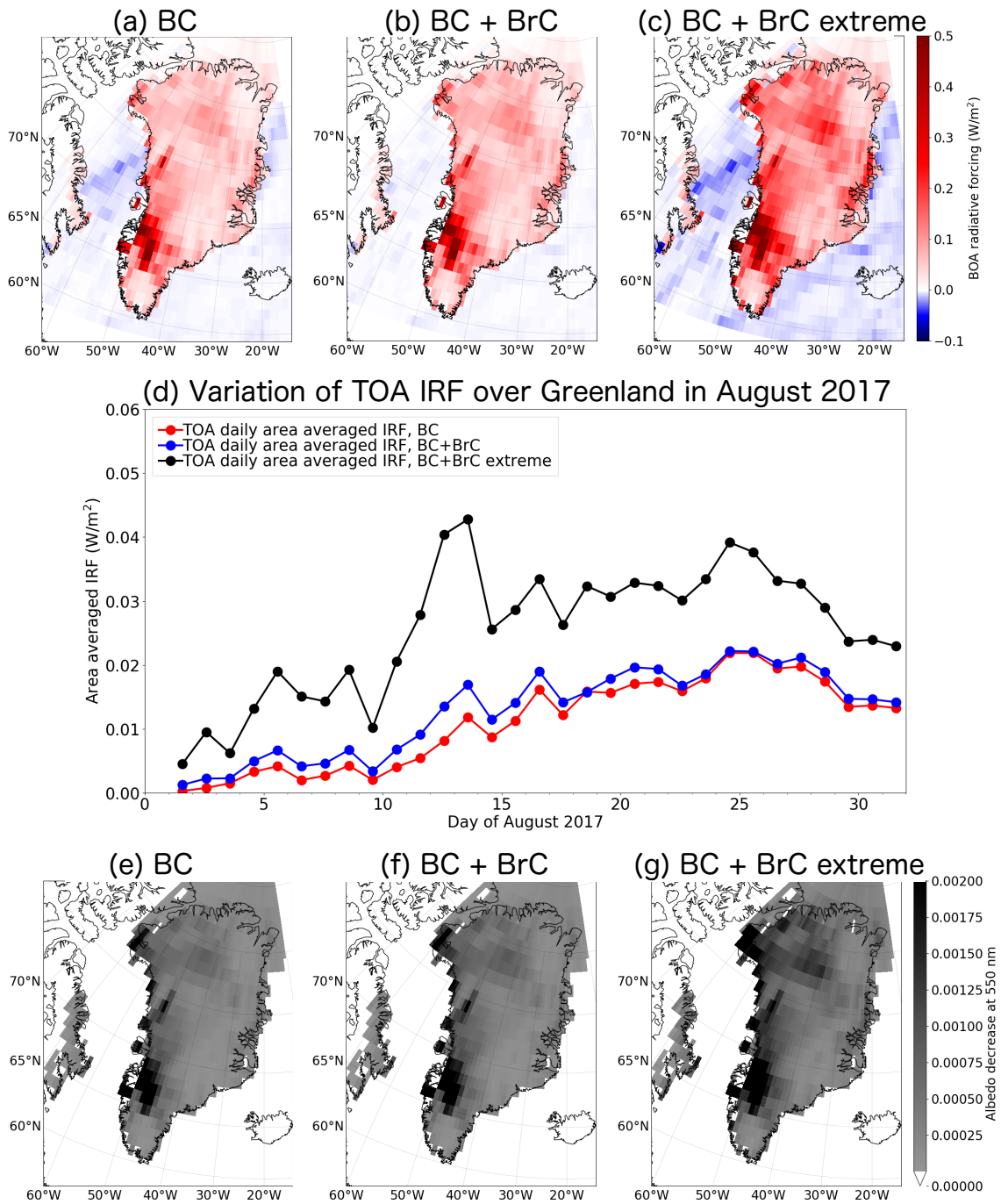
1066



1068

1069 **Figure 6.** (a) Worldview application from the NASA/Goddard Space Flight Center Earth  
 1070 Science Data and Information System (ESDIS) project on 14 August 2017. (b) Vertical cross-  
 1071 section along satellite's route (red line in c) of total attenuated backscatter at a wavelength of  
 1072 532 nm obtained from the CALIOP lidar on 14 August 2017 at 6 UTC (black line denotes the  
 1073 orography of the area). (c) Column-integrated BC concentration simulated with FLEXPART  
 1074 (red line shows the path of the satellite). (d) Vertical distribution of BC concentrations with  
 1075 longitude as seen with FLEXPART (grey area denotes the orography of the area).

1076



1077

1078 **Figure 7.** The instantaneous direct BOA RF due to (a) BC only, (b) BC and BrC, and (c) BC  
 1079 and BrC when OC was assumed to be all BrC (extreme case) from the Greenland fire for  
 1080 cloudy conditions on 31 August, 2017. (d) Daily variation of the TOA IRF over Greenland in  
 1081 August 2017 for the three studied scenarios. Albedo reduction at 550 nm due to (e) BC only,  
 1082 (f) BC and BrC, and (g) BC and BrC when OC was assumed to be all BrC (extreme case).  
 1083 Note that the maximum albedo change due to deposited smoke is 0.00585 (BC only), 0.00590  
 1084 (BC+BrC) and 0.00670 (BC+BrC extreme).

1085 **SUPPLEMENTARY FIGURE LEGENDS**

1086

1087 **Figure S 1.** Annual number of active fires over Greenland during the last 17 years as seen  
1088 from NASA's MODIS satellite (product MSC14DL).

1089

1090 **Figure S 2.** Fire dynamics in Greenland for the August 2017 fires according to MODIS  
1091 (magenta dots show active fire hot spots from the MODIS MCD14DL product). Locations of  
1092 stations with AOD measurements from AERONET are also shown.

1093

1094 **Figure S 3.** Median injection heights (km above sea level – ASL; left panel) and distribution  
1095 of longitudinally integrated burned biomass (Tg) as a function of injection altitude (right  
1096 panel) calculated by PRMv2 for the period between 31 July and 21 August 2017.

1097 **Figure S 4.** Dry to total deposition ratio (example for BC) from the 2017 peat fires over  
1098 Greenland.

1099

1100 **Figure S 5.** Relative standard deviation of deposited mass (example for BC) for different  
1101 assumed size distributions normalized against the results from our reference size distribution  
1102 with a logarithmic mean diameter of 0.25  $\mu\text{m}$ . Particle size distributions with aerodynamic  
1103 mean diameters of 0.1, 0.25, 0.5, 1, 2, 4, 8  $\mu\text{m}$  and a logarithmic standard deviation of 0.3  
1104 were simulated.

1105

1106 **Figure S 6.** Footprint emissions sensitivities for Northwestern, Northeastern, Southwestern  
1107 and Southeastern Greenland for the period 31 July to 31 August 2017. Active fires from  
1108 NASA's MODIS MCD14DL product are shown with red dots.

1109

1110 **Figure S 7.** Average contribution of biomass burning (upper panels) and anthropogenic  
1111 emissions (lower panels) to surface concentrations of (a) BC and (b) OC in Northwestern,  
1112 Northeastern, Southwestern and Southeastern Greenland (in  $\text{ng m}^{-3}$  per grid cell). Numbers (in  
1113 red) represent total concentrations in the studied domain, obtained by spatial integration over  
1114 all source grid cells. Receptor areas in Greenland are highlighted by pink boxes.

1115

1116 **Figure S 8.** (a) The single scattering albedo (SSA) of BC as a function of wavelength for  
1117 various modified combustion efficiencies (MCE). The star and dot marked lines are from the  
1118 parameterization of Pokhrel et al. (2016). (b) The IRF as a function of BC deposited on the  
1119 Ice Sheet. The calculations were made for cloudless conditions with a snow-covered surface  
1120 for noon on 31 August 2017 at 65°N.

**Table 1.** Start and end date of releases, source of data, type of sensor, burned area and daily increment of burned area, fuel consumption and calculated BC emissions from Eq. 1 during the Greenland fires in 2017. Total numbers for burned area, fuel consumption and BC emissions are highlighted in bold.

<b>Start</b>	<b>End</b>	<b>Source of RS data</b>	<b>Type of sensor</b>	<b>Burned area (ha)</b>	<b>Increment of burned area (ha)</b>	<b>Fuel consumption (t C)</b>	<b>BC emissions (kg)</b>	<b>OC emissions (kg)</b>	<b>BrC emissions (kg)</b>
31/07/17	02/08/17	Sentinel 2A	MSI	304	304	15176	3035	94543	18211
02/08/17	03/08/17	Landsat 8 OLI	MSI	428	125	6247	1249	38916	7496
03/08/17	04/08/17	Sentinel 1A	SAR	588	160	7980	1596	49712	9575
04/08/17	05/08/17	Sentinel 1A	SAR	740	152	7621	1524	47479	9145
05/08/17	07/08/17	Sentinel 2A	MSI	1100	359	17966	3593	111925	21559
07/08/17	08/08/17	Sentinel 2A	MSI	1314	214	10706	2141	66698	12847
08/08/17	12/08/17	Landsat 8 OLI	MSI	1868	554	27714	5543	172658	33257
12/08/17	14/08/17	Sentinel 1A	SAR	2005	136	6817	1363	42470	8180
14/08/17	15/08/17	Sentinel 1A	SAR	2169	165	8244	1649	51363	9893
15/08/17	16/08/17	Sentinel 1A	SAR	2209	40	1998	400	12444	2397
16/08/17	19/08/17	Sentinel 1A	SAR	2254	44	2213	443	13784	2655
19/08/17	21/08/17	Sentinel 2A	MSI	2345	92	4579	916	28530	5495
<b>TOTAL</b>					<b>2345</b>	<b>117259</b>	<b>23452</b>	<b>730524</b>	<b>140711</b>

RS - Remote Sensing

MSI - Multispectral Images

SAR - Synthetic Aperture RADAR

